LBL-7069
UC-70

Preliminary Thermal and Thermomechanical Modeling for the Near Surface Test Facility Heater Experiments at Hanford

VOLUME I

Tin Chan and Janet S. Remer
Earth Sciences Division

December 1978

Prepared for the U. S. Department of Energy
under Contract W-7405-ENG-48
and for Rockwell Hanford Operations —
a Department of Energy Prime Contractor —
under Memorandum Order No. W8A-SBB-51760

LBL-7069

PRELIMINARY THERMAL AND THERMOMECHANICAL MODELING FOR THE NEAR SURFACE TEST FACILITY HEATER EXPERIMENTS AT HANFORD

Volume 1

Tin Chan and Janet S. Remer

Earth Sciences Division
Lawrence Berkeley Laboratory
University of California
Berkeley, California 94720

December 1978

Prepared for the U.S. Department of Energy
under Contract No. W-7405-ENG-48
and for Rockwell Hanford Operations
-A Department of Energy Prime Contractor-
under Memorandum Order No. W8A-SBB-51760

Contents: Volume 1

Preface. v

List of Figures. vi

List of Tables xi

Acknowledgments. xiii

Abstract xv

1.0 Introduction. 1
1.1 Background and objectives. 1
1.2 Scope of present work. 2

2.0 Physical Systems to be Modeled. 4
2.1 Full-scale heater experiments. 5
2.2 Time-scaled heater experiment. 9

3.0 Thermal and Thermo-Mechanical Models Used 15
3.1 Closed form integral solutions for thermal analysis. . . 15
3.2 Finite element thermo-mechanical models 18

4.0 Results and Discussion. 22
4.1 Full-scale experiments 22
4.1.1 Temperatures. 24
4.1.2 Displacements 38
4.1.3 Stresses. 49
4.1.4 Interference of the two full-scale experiments. . 58
4.2 Time-scaled experiment 65

5.0 Summary, Conclusions and Recommendations. 73

References 79

Appendix A: Closed Form Integral Solutions for Temperature Distribution Due to a Finite Cylinder and a Disc Source with Arbitrary Time Dependence. 83

Appendix B: Generalization to an Anistropic Medium. 87

Appendix C: Consideration of Temperature Rise as a Function of the Group Parameter t/r^2; Comparison of Finite Line and Infinite Line Sources 89

Appendix D tables: Table D1, Summary of Figures Representing Models Studied
Table D2, Correspondence between Figures in Volume 1 and Appendix D, Volume 2. 93

PREFACE

This report documents the detailed results of the pre-design thermomechanical calculations for the heater tests at the Near Surface Test Facility at Hanford, in partial fulfillment of the FY 78 Statement of Work funded through Rockwell International Order Number W8A-SBB-51760. The results of this study have been used in the design of the heater experiments. An extended summary of this report, containing results for two out of the six cases considered for the full-scale tests, has been included in DuBois et al. (1979).

This report is published in two volumes. Volume 1 contains a description of the proposed experiments, the theoretical models investigated, and an analysis of the results. Because the inclusion of all of the figures produced would make this report too unwieldly, only a selection of figures, intended to illustrate important results, has been included in Volume 1. Volume 2, available through the National Technical Information Service in Virginia, contains the complete set of figures, which provides the detailed information necessary to design the heater experiments.

LIST OF FIGURES

		Page
Figure 1	Hanford Full-Scale Experiment Heater Array	6
Figure 2	Hanford Full-Scale Experiment Power Schedules	8
	(a) Power Schedule 1a (b) Power Schedule 1b (c) Power Schedule 1c (d) Power Schedule 2a (e) Power Schedule 2b (f) Power Schedule 2c	
Figure 3	Hanford Time-Scaled Experiment Heater Array	12
Figure 4	Hanford Time-Scaled Experiment, Power Schedule 3	13
Figure 5	Finite Element Mesh and Boundary Conditions for Full-Scale Heater Experiment	19
	(a) View of entire finite element mesh (b) Details of area "B" in "A" (c) Details of area "C" in "B"	
Figure 6	Temperature Profiles for Hanford Full-Scale Experiment: $z = 0.0$ m, $\theta = 0^{o}$, $r = 0.203$ to 0.881 m	25
	(a) Power Schedule 1a (b) Power Schedule 2a (c) Power Schedule 2c	
Figure 7	Temperature Profiles for Hanford Full-Scale Experiment: $z = 0.0$ M, $\theta = 0^{o}$, $r = 0.919$ to 5.0 m	27
	(a) Power Schedule 1a (b) Power Schedule 2a (c) Power Schedule 2c	
Figure 8	Isotherms in Vertical Plane, Hanford Full-Scale Experiment: Infinite Medium Model, Main Heater = 5 kW	34
	(a) 365 days (b) 730 days	

		Page
Figure 9	Isotherms in Vertical Plane, Hanford Full-Scale Experiment: Isothermal Boundary Model, Main Heater = 5 kW (a) 30 days (b) 365 days (c) 730 days	35
Figure 10	Isotherms in Vertical Plane, Hanford Full-Scale Experiment: Infinite Medium Model, 2-kW Main Heater (a) 365 days (b) 730 days	36
Figure 11	Isotherms in Vertical Plane, Hanford Full-Scale Experiment: Isothermal Boundary Model, 2-kW Main Heater (a) 30 days (b) 365 days (c) 730 days	37
Figure 12	Deformation of Heater Drift and Borehole under Power Schedule 1a, Hanford Full-Scale Experiment (a) 730 days (b) 1095 days	39
Figure 13	Displacement Profiles (u_z) for Mesh 7, 730 days, Hanford Full-Scale Experiment (a) r = 0.45 m (b) r = 1.875 m (c) r = 10.5 m	43
Figure 14	Displacement Profile (u_r) for Mesh 1, Hanford Full-Scale Experiment. Main Heater = 5 kW; z = 0.0 m; $\theta = 0^o$ (a) 30 days (b) 90 days (c) 180 days (d) 365 days (e) 371 days (f) 730 days	46
Figure 15	Displacement Profile (u_r) for Mesh 7, Hanford Full-Scale Experiment. Main Heater = 5 kW; z = 0.0 m, $\theta = 0^o$; 730 days.	48

		Page
Figure 16	Stress Profiles for Mesh 1, Hanford Full-Scale Experiment. Main Heater = 5 kW; z = 0.0 m, $\theta = 0^{o}$ (a) 1 day (b) 7 days (c) 30 days (d) 365 days (e) 371 days	51
Figure 17	Tangential Stress Along Floor of Heater Drift (z = 3.875 m), Hanford Full-Scale Experiment. Mesh 7, 730 days	54
Figure 18	Radial Stress Along Floor of Heater Drift (z = 3.875 m), Hanford Full-Scale Experiment. Mesh 7, 730 days	55
Figure 19	Interference Between the Two Full-Scale Experiments: Combined Temperature Profile at z = 0 m, $\theta = 0^{o}$; Infinite Medium Model; 730 days	60
Figure 20	Interference Between the Full-Scale Experiments: Stress (σ_r) Profiles at z = 0 m, $\theta = 0^{o}$; Mesh 1, 730 days	61
Figure 21	Interference Between the Two Full-Scale Experiments: Displacements (u_r) Profiles at z = 0 m, $\theta = 0^{o}$; Mesh 1, 730 days	62
Figure 22	Quarter Plane Showing Locations at Which Temperature Profiles Were Made, Hanford Time-Scaled Experiment	66
Figure 23	Temperature Profiles for Hanford Time-Scaled Experiment (a) x = 8.75 to 14 m, y = 0 m, z = 0 m (b) x = 0.045 to 3.455 m, y = 0.045 to 1.455 m, z = 0 m	68
Figure 24	Isotherms in Horizontal Plane, Hanford Time-Scaled Experiment, z = 0 (a) 7 days (b) 90 days (c) 180 days (d) 365 days (e) 730 days	69

		Page
	(f) 737 days (g) 910 days (h) 1095 days	
Figure 25	Migration of 5° Isotherm in Horizontal Plane, Hanford Time-Scaled Experiment	72
Figure C1	Comparison of Temperature Profiles for Infinite and Finite Line Sources	90

LIST OF TABLES

		Page
Table 1a	Dimensions of the Full-Scale Heater Experiments	7
Table 1b	Power Levels of the Central Heater for the First Two Years of the Full-Scale Experiments	7
Table 2	Material Properties Used	14
Table 3	Summary of Figure Numbers Representing Models Studied	23
Table 4	Calculated Temperature Rise (°C) at the End of the First, Second and Third Years of the Full-Scale Experiments	29
Table 5	Significant Temperature Values and Predicted Times at Which the Temperature is Attained (Full-Scale Experiments) for an Infinite Medium Model	31
Table 6	Maximum Predicted Vertical Displacement, u_z, 0.375 m Below the Floor of the Heater Drift (Full-Scale Experiments), Mesh 1 and Mesh 7	41
Table 7	Maximum Predicted Vertical Displacement, u_z, at Various Radial Distances (Full-Scale Experiments), $\theta = 0^o$.	44
Table 8	Maximum Predicted Radial Displacement, u_z, in the Midplane (Full-Scale Experiments)	47
Table 9	Maximum Predicted Compressive Stresses in the Heater Midplane (Full-Scale Experiments) for Mesh 1, $\theta = 0^o$.	52
Table 10	Maximum Predicted Stresses 0.375 m Below the Floor of the Heater Drift (Full-Scale Experiment), Mesh 7	56
Table 11	Predicted Combined Radial Displacements, u_r, in the Heater Midplane of the Two Full-Scale Experiments, Mesh 1	64

ACKNOWLEDGMENTS

The authors would like to acknowledge the assistance of J. S. Kuo and O. Wan in computer programming, and J. A. Jeffry and S. Peterson for plotting some of the graphs. We would also like to thank C. Miller for her constructive comments and N. G. W. Cook for his helpful discussions with T. Chan on *in situ* heater experiments.

ABSTRACT

Preliminary thermal and thermomechanical analyses have been carried out for the heater experiments in the Near Surface Test Facility at Gable Mountain on the Hanford Reservation, Richland, Washington. Temperatures were calculated by Green's function method for the full-scale and time-scaled experiments. Six different heater power schedules were considered for the full-scale experiments to bracket all possible values of initial spent fuel power from canisters buried after different periods of cooling. Linear elastic finite-element models were used to calculate the thermally induced displacements and stresses for two of the power schedules. Due to the poor thermal conductivity and rather high Young's modulus of Pomona basalt (the rock type in which the heater experiments are to be conducted), very high temperatures, displacements and stresses were predicted in spite of the relatively low thermal expansion coefficient. These predicted values have been used for the design of the experiments. Recommendations are made in this report regarding the conduct of the experiments and the interpretation of the field data, as well as further thermomechanical modeling and input data required for more meaningful modeling of a fractured rock mass. Equations are given in Appendices A and B for temperatures caused by an arbitrary time-dependent cylindrical heater of finite length and radius, a finite-radius disc heater, as well as the generalization to the situation of an anisotropic medium.

1. INTRODUCTION

1.1 Background and objectives

In assessing the feasibility of a potential site for underground storage of nuclear waste, the ultimate question is whether the rock barrier can prevent the radioactive material from returning to the biosphere before it has decayed to an acceptably low level of toxicity. An important difference between a radioactive waste repository and other underground excavations is the thermal loading imposed on the host rock by the heat released from radioactive decay. Long-term isolation is affected because the thermo-mechanical perturbation may reduce the total compressive stress or even lead to crack opening, thereby increasing the permeability of the rock mass. Furthermore, the temperature gradient may also cause thermal convection of ground water. In the near term, the thermo-mechanical response of the rock mass around the canisters and the excavation must be understood in order to facilitate design and control, to assure accessibility and retrievability.

Since the nuclear waste has to be isolated for a period on the order of a million years, one can only rely upon mathematical models to predict the possible consequences. A prerequisite for any model used for such predictions is that it be able to correctly predict the thermomechanical response of the rock mass on the canister and excavation scales during the operating (retrievable) period of the repository. Because there has been little experience in the effects of temperature on rock mass behavior, especially in hard rocks, it is necessary to run in situ simulation tests using electrical heaters

in a geological environment similar to a potential site before actual waste canisters are emplaced.

One such test is the Near-Surface Test Facility (NSTF) heater experiments in the Pomona Basalt Flow in Gable Mountain on the Hanford Reservation, Richland, Washington (Rockwell Hanford Operations, 1978). The thermo-mechanical modeling presented in this report is part of Lawrence Berkeley Laboratory's (LBL) contribution to the project. The preliminary temperature, displacement and stress results have been used for the design of heaters and the layout of instrumentation. The original plan was that data from the heater experiments would be analyzed by comparison with the model predictions. This would enable the model to be progressively refined. The validated model would then be used in the repository design. By continually monitoring the repository during the initial period of operation, testing the field data against the models and modifying the models if necessary, it was hoped that viable models would evolve that could be used with some confidence to predict the long-term thermomechanical response of a rock mass (e.g., basalt) containing fractures.

1.2 Scope of present work

The work reported here includes thermal conduction calculations for all three heater experiments using closed form integral solutions and thermomechanical calculations for the full-scale tests (see Section 2) using linear elastic finite element models. After the completion of the present calculations, design changes were made, partly on the basis of the theoretical results. Consequently, the results contained in this report do not reflect the latest design changes. Similar models have

been used previously to predict the temperatures, displacements and stresses for the Stripa Heater Project (Chan et al., 1978; Chan and Cook, 1979). Preliminary field data (Cook and Hood, 1978) have corroborated the predicted temperatures.

The configurations and power schedules of the heater experiments modeled are described in Section 2. Each heater experiment is modeled as an array of finite-length line heaters in an infinite or semi-infinite medium. Section 3 summarizes the equations obtained by means of Green's functions and image methods for the temperature rise due to such an array, as well as the finite-element model for the thermoelastic calculations. Section 4 contains the numerical results and Section 5, a summary along with conclusions and recommendations. In addition, four appendices have been included. Appendix A gives the closed form integral solutions for an arbitrary time-dependent finite-length, finite-radius cylinder source and finite-radius disc. These solutions should be useful for repository-scale modeling. In Appendix B, the generalization of the preceding solutions to the case of an anisotropic medium is briefly discussed. Appendix C discusses the inappropriateness of examining the predicted temperature as a function of t/r^2 and compares the temperature solutions generated by finite line and infinite line sources.

Only representative figures have been included within the main text of this report to illustrate the major results. A complete set of full-size graphs is contained in Appendix D (Volume 2, available from NTIS in Virginia) for the benefit of readers who would like to read numerical values from the graphs. Wherever a figure number is given in the text, it is followed by the equivalent Appendix D figure number is enclosed in square brackets.

2. PHYSICAL SYSTEMS TO BE MODELED

The heater experiments to be modeled consist of two full-scale tests and a time-scaled test, essentially an adaptation of concepts utilized in the Stripa Heater Project (Cook and Witherspoon, 1978). Each type of experiment will provide information on a different aspect of the design of a nuclear waste repository. The full-scale tests will be used to obtain quantitative data about the short-term response of basalt to the thermal loading imposed by a buried heat source. With this in mind, the central heaters used in the full-scale experiments will be designed to approximate waste canisters in size and heat generation. (Actually the central heater canister in these experiments has approximately the same size as high-level reprocessed waste. Spent fuel rods will have different sizes unless they are re-packaged.) Each central heater will correspond to a different age of spent fuel.

Due to the low thermal conductivity and diffusivity measured in samples of basalt taken from the NSTF, it is expected that the rock within a short distance of the heaters will approach its maximum temperature within a few months. One possible consequence of an extreme thermal loading is borehole decrepitation which, it if does occur, will be observable during the experiment. Therefore, within a short period of time, the full-scale experiment should provide investigators with information to determine the thermal and stress tolerance of in situ basalt.

The purpose of the time-scaled experiment is to study the long-term effects of an array of buried heat sources. It is important for repository design that an understanding be developed of the temperature

distribution surrounding a heat source array, and of the interactions between individual heat sources.

Using the laws of heat conduction, a three-year experiment involving 1.125-kW heaters can be used to model the temperature distribution of an array of full-size 3.6-kW canisters during a thirty-year period. The details involved in the scaling are explained in Section 2.2.

A brief description of the heater arrangements is given below. Further details can be found in the "In Situ Heater Experiment Plan" (Rockwell Hanford Operations, 1978).

2.1 Full-scale heater experiments

Each full-scale experiment consists of a central heater surrounded by a ring of eight peripheral heaters as illustrated schematically in Fig. 1 [D1], which also shows the cylindrical coordinate system used in the calculations. This heater array is placed in holes drilled from the floor of the heater drift such that the mid-plane of the heaters is approximately 14 feet (4.25 m) below the floor. The central heater simulates the local thermo-mechanical effects of a waste canister and the peripheral heaters simulate the rise of ambient temperature caused by other canisters in a repository. Dimensions of the heaters and holes are given in Table 1a.

Six different power levels and schedules have been considered in the thermal calculations to bracket all reasonable possibilities. These are shown in Figs. 2a-2f [D2a-D2f]. The power schedule of the central heater is best described as a series of step functions, whereas the power output by the peripheral heaters is constant for the whole period of time that they are on.

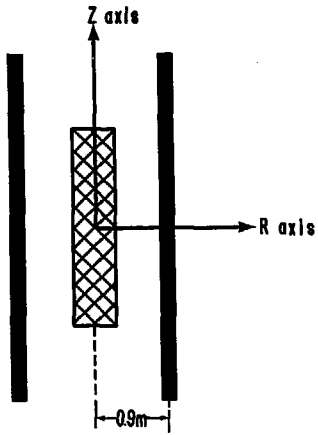

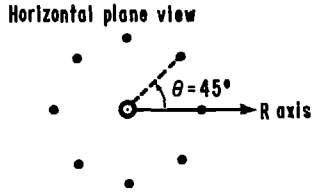

⊙ Central (main) heater :
length = 2.4384 m (8 ft.), radius = 0.2286 m (9 in)
energized at start of experiment.

• Peripheral heaters :
length = 4.2672 m (14 ft), radius = 0.0191 m (0.75 in) ;
energized 365 days after start of experiment

Axes represented are those used in numerical modeling.

Diameters of heaters in diagram are greately exaggerated.

XBL 787-1993

Figure 1 Hanford Full-Scale Experiment Heater Array

Table 1a. Dimensions of the full-scale heater experiments.

Length of central heater canister = 8.5 ft (2.59 m)
Length of heater element = 8 ft (2.44 m)
Diameter of central heater canister = 12.75 in. (0.324 m)
Diameter of central heater hole = 18 in. (0.457 m)
Length of peripheral heater = 14 ft (4.27 m)
Diameter of peripheral heater hole = 3 in. (0.038 m)
Radius of the ring of peripheral heaters = 35.4 in. (0.9 m)
Center-to-center separation between the two experiments = 68.9 ft (21 m)

Table 1b. Power levels of central heater for first two years of the full-scale experiment.

Power Schedule	0 to 180 days	180 to 730 days
1a (Fig. 2a)	5 kW	5 kW
1b (Fig. 2b)	2.5 kW	5 kW
1c (Fig. 2c)	2.5 kW	2.5 kW
2a (Fig. 2d)	2 kW	2 kW
2b (Fig. 2e)	1 kW	2 kW
2c (Fig. 2f)	1 kW	1 kW

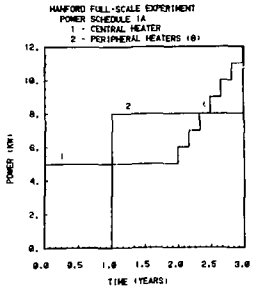

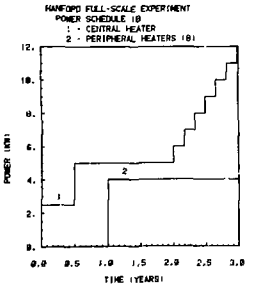

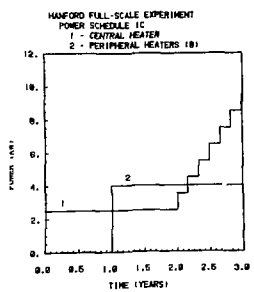

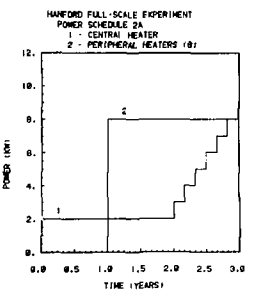

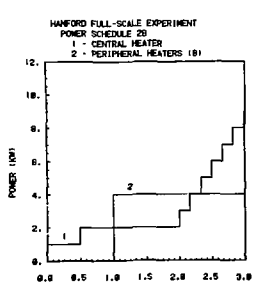

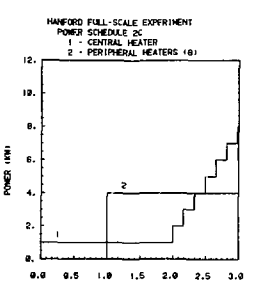

Figure 2 Hanford Full-Scale Experiment Power Schedules

The power schedules have been divided into two groups based on the power level of the central heater. The central heater for power schedules in the first group (1a, 1b, 1c) has an initial power of either 5 kW or 2.5 kW. The 5-kW heater corresponds to the power generated by a PWR (Pressurized Water Reactor) spent fuel assembly approximately one year after discharge from a reactor and the 2.5-kW heater corresponds to the same spent fuel assembly approximately two years after discharge (Llewellyn, 1978). The central heater in the second group has an initial power of either 2 kW or 1 kW, corresponding to a PWR spent fuel assembly 2.5 and 4.5 years after discharge, respectively (Llewellyn, 1978). The power levels of the main heater for the first two years of the experiment are given below in Table 1b.

The peripheral heaters are energized one year after the start of the experiment and their power levels are held constant at either 0.5 kW per peripheral heater (1b, 1c, 2b, 2c) or 1 kW per peripheral heater (1a, 2a).

After the experiments have been running for two years, the overload test begins. This consists of an increase of 1 kW to the power level of the central heater every 60 days until the end of the experiment one year later. At the end of the three years the highest central heater power level is 12 kW for power schedule 1a (Fig. 2a [D2a]) and the lowest is 8 kW for schedule 2c (Fig. 2f [D2f]).

2.2. Time-scaled heater experiment

The time-scaled experiment will simulate the interaction between adjacent nuclear waste canisters in a row and between rows in different storage tunnels in a repository for a period equivalent to approximately

30 years of repository operation time. This is based upon the laws of linear heat conduction which allows the time to be scaled down by a ratio equal to the square of the ratio of linear dimensions. To understand the basis of scaling one can either examine the form of the solutions (Cook and Witherspoon, 1978; Chan et al., 1978) or the heat diffusion equation itself. Thus, for simplicity, consider the one-dimensional homogeneous heat diffusion equation:

$$\frac{\partial T}{\partial t} = \kappa \frac{\partial^2 T}{\partial x^2}$$

where T = temperature, t = time, x = distance, and κ = thermal diffusivity. The solution of Eq. (1), T(x,t), gives the temperature distribution of a physical system (I) with spatial variable x and time variable t. Suppose one now has a physical system (II) described by spatial variable $x_d = x/L$ and time variable $t_d = t/L^2$ where L is some scale length, then the temperature distribution $T(x_d,t_d)$ of this system satisfies the equation obtained by substituting x and t in terms of x_d and t_d into Eq. (1):

$$\frac{\partial T}{\partial t_d} = \kappa \frac{\partial^2 T}{\partial x_d^2} \quad . \qquad (1)$$

Since equations (1) and (2) are identical, $T(x_d,t_d)$ for system II is equal to T(x,t) for system I.

Each heater of the time-scaled experiment is 2.66 ft (0.81 m) in length. Comparison with the length of a full-scale heater (2.59 m) gives a linear scale ratio of approximately 1:3.2 and therefore, a time scale ratio of $1:(3.2)^2 = 1:10.22$. The heaters are arranged

in a rectangular array at spacings of 3 m and 7 m (Fig. 3 [D3]), which corresponds to a in a 9 m by 21 m full-scale storage room. To simulate the effects of sequential step loading, an array of four secondary heaters will be turned on two years after the primary array.

Though the linear scale ratio has been determined by the ratio of heater lengths, it is important that the reduction of the linear scale must not be too extreme because geological structures such as fracture patterns cannot be scaled.

The initial power of each heater is 1.125 kW, which corresponds to a 3.6-kW full-scale canister, the heat output of a PWR of spent fuel assembly approximately 1.5 years after discharge from a reactor. Note that the time-scaled experiment will not be directly comparable to either of the full-scale experiments as currently proposed. However, the validity of the scaling has been shown by the Stripa Heater Project (Chan et al., 1978). In the preliminary calculations the power of the heaters is assumed constant (Fig. 4 [D4]). In a later calculation the power will be decayed according to the expected time variation of spent fuel heat production rate.

Material properties of the host rock, Pomona basalt, have been taken from laboratory measurements on small specimens (Martinez-Baez and Amick, 1978) for the thermal calculations and from mean literature values summarized by Agapito et al. (1978) for the thermo-mechanical calculations. These are listed in Table 2.

Horizontal plane view of arrangement of heaters.

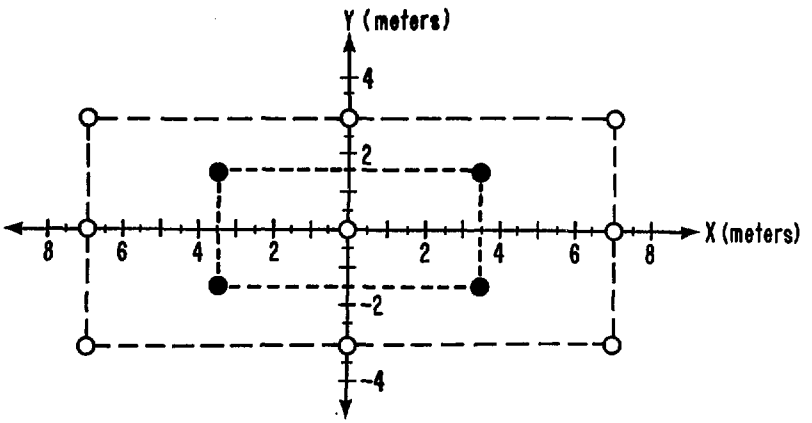

○ Primary heaters: length = 0.81 m; radius = 0.0635 m; energized at start of experiment.

● Secondary heaters: length = 0.81 m; radius = 0.0635 m; energized 730 days after start of experiment.

Axes represented are those used in numerical modeling.

Diameter of heaters in diagram is greatly exaggerated.

XBL 787-1994

Figure 3 Hanford Time-Scaled Experiment Heater Array

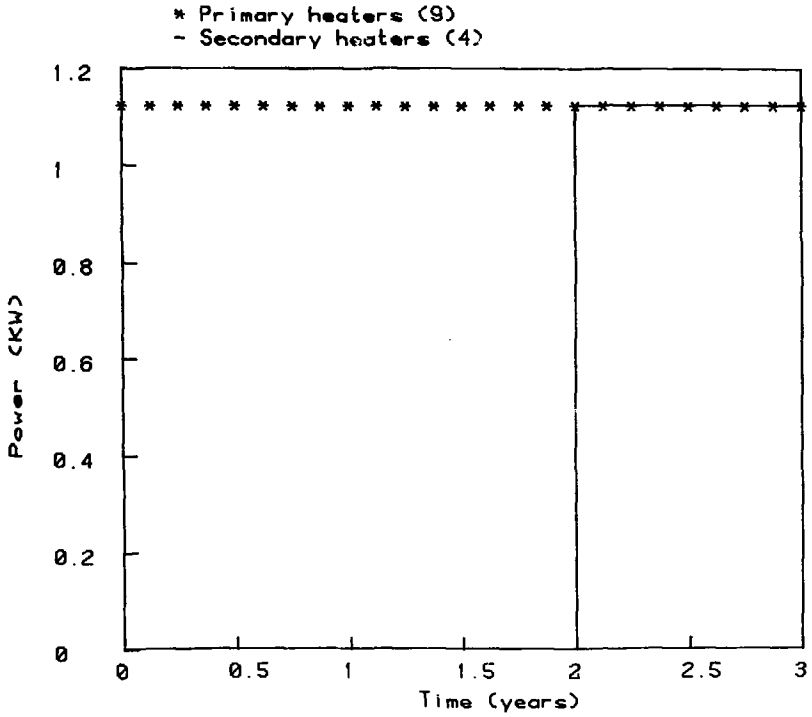

Figure 4 Hanford Time-Scaled Experiment, Power Schedule 3

Table 2. Material properties used.

Property	Symbol	Value
Density[a]	ρ	2865 kg/m^3
Specific heat[a]	c	1164 J/kg^{o}C
Thermal conductivity[a]	k	1.62 W/m^{o}C
Thermal diffusivity[a]	$\kappa = k/\rho c$	4.86 x 10^{-7} m^2/sec
Poisson's ratio[b]	ν	0.26
Thermal expansion coefficient[b]	α	5.4 x 10^{-6}/^{o}C
Young's modulus[b]	E	7 x 10^4 MPa

[a]Values used are "estimated thermal values at 200^{o}C" for Pomona basalt based on laboratory measurements at lower temperatures (Martinez-Baez and Amick, 1978).

[b]Average basalt properties (Agapito et al., 1978). Laboratory data for Pomona basalt (Duvall et al., 1978) was not yet available at the start of the present calculations. The elastic properties used are very similar to those measured by Duvall et al., while the thermal expansion coefficient is slightly lower than their laboratory result (6.6x10^{-6}/^{o}C). A higher thermal expansion coefficient would lead to proportionally higher displacements and stresses.

3. THERMAL AND THERMO-MECHANICAL MODELS USED

3.1 Closed form integral solutions for thermal analysis

The Green's function method (Morse and Feshbach, 1953) has been used to obtain closed form integral solutions to the heat transfer problem for the heater experiments. Here the term Green's function is used in accordance with the terminology of applied mathematicians, i.e., it includes the point source method (also known as singularity solution or impulse response) as well as boundary integrals. This technique for solving nonhomogeneous linear partial differential equations is well-known among mathematical physicists and engineers and has been applied to a wide variety of physical problems ranging from electrostatics (Jackson, 1975) through wave propagation (Morse and Feshbach, 1953) and heat diffusion (Carslaw and Jaeger, 1959) to quantum statistical mechanics of electron states in liquid metals (Chan and Ballentine, 1971).

The physical situation in the heater experiments is amenable to this method of solution with the following approximations:

(i) conduction is the only mode of heat transfer;

(ii) the heaters and the rock medium are both homogeneous, isotropic and have the same constant (temperature-independent) thermal properties;

(iii) the heaters are in direct thermal contact with the rock;

(iv) the rock medium can be considered infinite with uniform initial temperature or semi-infinite with the heater drift idealized as an isothermal or adiabatic boundary.

Under these assumptions the problem can be handled with the point source method, a particular case of the Green's function method.

In view of the short thermal diffusion time across the radius of the heater and its small heat capacity compared with that of the rock volume to be heated up, the heater can be represented by a finite line source. The validity of this approximation has been verified by numerical comparison between the finite line source and the finite cylinder source solutions (Chan et al., 1978). The temperature rise ΔT at a point (x,y,z) at time t due to a line source of power per length Q_l and length 2b, located along the z-axis so that the mid-point of the heater is at the origin of the coordinate system, can be shown (Chan et al., 1978) to be

$$\Delta T(x,y,z,t) = \frac{1}{8\pi k} \int_0^t Q_l(t-\mu) \left[\operatorname{erf}\left\{ \frac{z+b}{2(\kappa\mu)^{1/2}} \right\} - \operatorname{erf}\left\{ \frac{z-b}{2(\kappa\mu)^{1/2}} \right\} \right] \frac{1}{\mu} \exp \frac{-r^2}{4\kappa\mu} \, d\mu \quad , \tag{3}$$

where $r^2 = x^2 + y^2$, k = thermal conductivity, and κ = thermal diffusivity.

The effect of a plane adiabatic or isothermal boundary can be simulated with positive or negative images, respectively. The total temperature rise due to an array of H parallel line heaters in a semi-infinite medium can be obtained by superimposing the temperature rise caused by each, giving

$$\Delta T_{total}(x,y,z,t) = \sum_{h=1}^{H} \Delta T_h(r_h, z-z_h, t-t_h | Q_h, b_h) + \sum_{h=1}^{H} \Delta T_h(r_h, z-2z_o+z_h, t-t_h | \pm Q_h, b_h) \quad (4)$$

where ΔT_h = temperature rise due to the h^{th} heater

$2b_h$ = length of the h^{th} heater

Q_h = power per unit length of the h^{th} heater

(x_h, y_h, z_h) = coordinates of the mid-point of the h^{th} heater

$r_h^2 = (x-y_h)^2 + (y-y_h)^2$

t_h = turn-on time of the h^{th} heater

z_o = elevation of the plane boundary

and all the heaters are oriented parallel to the z-axis. In the case of an infinite medium only the first term of Eq. (4) needs to be considered. For all the three heater experiments being modeled, $z_h = 0$ for all heaters.

In the case of the full-scale experiments, temperatures were calculated for the various power schedules for both the infinite medium model and the isothermal boundary model, with the temperature assumed to remain constant on a plane at the elevation of the heater drift floor. In a previous work (Chan et al., 1978) it was found, by comparison with a fully numerical model where Newton's law of cooling was assumed at the boundary of the drift, that the true temperature should lie somewhere between the two previously mentioned idealizations. For the time-scaled experiment only the infinite medium model has been used since the mid-plane of the heater array is 10 m below the drift floor and the influence of the drift is, therefore, not expected to be significant as far as temperatures are concerned. It should

be noted that all the thermal models are three-dimensional although the results are presented in plane sections.

3.2 Finite-element thermo-mechanical models

Thermally induced displacements and stresses were calculated using the finite-element program SAPIV (Bathe et al., 1974). The LBL-LLL version of SAPIV (Sackett, unpublished) incorporates a bandwidth minimizer and a COMPASS (CDC assembly language) subroutine for dynamic core allocation to allow effective use of small and large core memory spaces. Our temperature program FILINE (based on the method described in Section 3.1) has been interfaced with SAPIV for thermo-mechanical analysis. Linear thermoelasticity is assumed by the program.

In the present calculations the rock medium is further approximated as a homogeneous, isotropic continuum. This is necessary only because of lack of data on *in situ* rock mass properties and conditions. Actually the finite-element method is well suited for heterogeneities and the SAPIV program can handle orthotropic, temperature-dependent material properties.

In constructing the finite element models for the full-scale experiments two other approximations were introduced:

(i) the system is axially symmetric about the axis of the central heater, and

(ii) the mid-plane of the heater array is a plane of symmetry.

Two finite element meshes have been used. The first (hereafter referred to as Mesh 1), comprising 651 nodes and 607 4-node isoparametric quadrilateral elements, considers the rock medium (except the central heater hole) as an infinite medium. Figures 5a-c [D5a-D5c] illustrate the

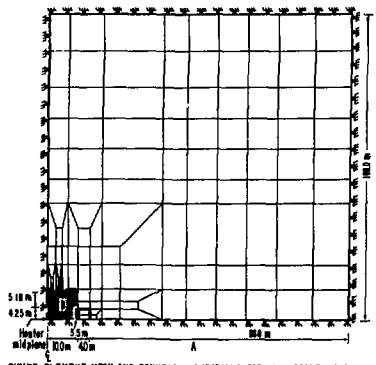

(a) FINITE ELEMENT MESH AND BOUNDARY CONDITIONS FOR FULL SCALE HEATER EXPERIMENT 2.

XBL 796-1963A/B

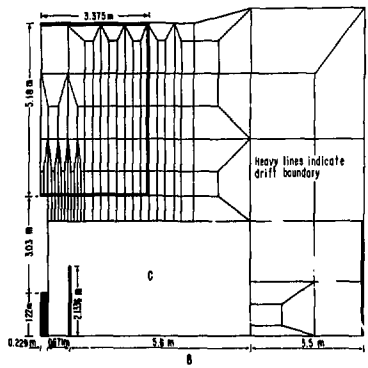

(b) DETAILS OF AREA "B" IN "A".

XBL 796-1964/B

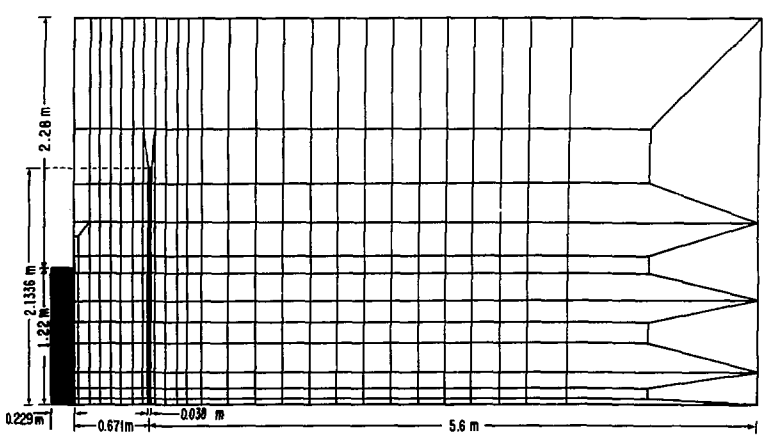

(c) DETAILS OF AREA "C" IN "B".

XBL 796-1965A/B

Figure 5 Finite Element Mesh and Boundary Conditions for Full-Scale Heater Experiment

mesh pattern at three different levels of detail. In the second mesh (hereafter referred to as Mesh 7) the elements within the heater drift and extensometer drift, as indicated by heavy lines in Figs. 5a [D5a] and 5b [D5b], are removed. Zero normal displacement boundary conditions were applied to the outer horizontal and vertical boundaries of the model block. Previous work (Chan and Cook, 1978) has confirmed that the fixed boundaries are sufficiently remote from the region where substantial temperature changes occur so that the thermally induced displacements and stresses are practically the same as those obtained using alternative boundary-loading conditions. The alternative analysis for comparison was carried out in the following manner. First a finite-element analysis was performed by applying assumed horizontal and vertical virgin stresses to the appropriate outer boundaries of the model with the drifts excavated (Mesh 7). In addition, gravity was applied as a body force to each element. Within the realm of linear elasticity this yields the mechanical displacements, u_i^{mech} and stresses, σ_{ij}^{mech} ,

$$u_i^{mech} = u_i^{vir} + u_i^{exc} \quad , \quad i = 1,2,3 \quad , \tag{5}$$

$$\sigma_{ij}^{mech} = \sigma_{ij}^{vir} + \sigma_{ij}^{exc} \quad , \quad i,j = 1,2,3 \tag{6}$$

where

u_i^{vir} = displacement (spurious) in the rock continuum caused by applying the virgin stresses as boundary loads and gravity,

u_i^{exc} = displacement induced by excavations,

σ_{ij}^{vir} = stress in the rock continuum caused by applying the virgin stresses as boundary loads and gravity,

σ_{ij}^{exc} = stress induced by excavations.

Next, a second run was made with thermal loading added. The total displacement u_i^{tot} and total stress would be σ_{ij}^{tot}:

$$u_i^{tot} = u_i^{vir} + u_i^{exc} + u_i^{th} \quad , \tag{7}$$

$$\sigma_{ij}^{tot} = \sigma_{ij}^{vir} + \sigma_{ij}^{exc} + \sigma_{ij}^{th} \quad . \tag{8}$$

Hence, the thermally induced displacements and stresses are obtained by taking the difference

$$u_i^{th} = u_i^{tot} - u_i^{mech} \quad , \tag{9}$$

$$\sigma_{ij}^{th} = \sigma_{ij}^{tot} - \sigma_{ij}^{mech} \quad . \tag{10}$$

The results were found to be in close agreement with those obtained using zero normal displacement boundary conditions.

In the geological environment of the Hanford NSTF the validity of the zero vertical displacement boundary condition for the top boundary requires further confirmation since the experiment horizon is only about 50 m below the surface. A proper analysis can be undertaken with the surface of the earth as a free boundary but also requires the measured virgin state of stress (which was not available at the time these calculations were made) as input. The frequently used relation

$$\sigma_h = \frac{\nu}{1-\nu} \sigma_v \quad ,$$

where

σ_h = horizontal virgin stress,

σ_v = vertical virgin stress,

ν = Poisson's ratio,

is unlikely to be valid since it applies only to uniaxial strain condition which may not hold at the NSTF site in view of the presence of a cliff and slope.

4. RESULTS AND DISCUSSION

This section contains the numerical results that have been used to design the two full-scale experiments and the time-scaled experiments. The calculations predict temperature rise in the time-scaled experiment and temperature rise, displacement, and stress in the full-scale experiments. The results have been presented as tables and graphs.

Table 3 contains a summary of the calculations and the corresponding figure numbers of the resulting plots made for this report. It shows the type of calculation (temperature, displacement, or stress) made for every combination of power schedule with mathematical model.

4.1 Full-scale experiments

A cylindrical polar coordinate system has been used for the geometry of the full-scale experiment. The z-axis lies along the vertical axis of the central heater with its origin located at the center of the central heater (Fig. 1a). The positive direction is towards the floor of the heater drift (or surface of the earth). The polar angle θ is defined such that a radial vector passing through

Table 3. Figure numbers representing models studied.

FULL-SCALE EXPERIMENTS						
	Temperature Calculations		Displacement Calculations		Stress Calculations	
Power Schedule	Infinite Medium	Isothermal Boundary	Mesh 1	Mesh 7	Mesh 1	Mesh 7
1a (Fig. 2a)	6a,7a 8a,8b	9a-9c	12a,12b 14a-14f	12a,12b 13a-13c 15	16a-16e	17,18
1b (Fig. 2b)						
1c (Fig. 2c)						
2a (Fig. 2d)	6b,7b 10a,10b	11a-11c		13a-13c		17,18
2b (Fig. 2e)						
2c (Fig. 2f)	6c,7c					
Interference between experiments with 1a (Fig. 2a) and 2a (Fig. 2d)	19		21		20	
TIME-SCALED EXPERIMENTS						
3 (Fig. 4)	23a,23b 24a-24h 25					

the center of one of the peripheral heaters will have a polar angle equal to 0^{o} or some multiple of 45^{o} (Fig. 1b). From symmetry consideration, only values of θ in the range 0^{o} to 22.5^{o} are of interest. Most of the calculations, whose graphs are contained in this report, have been made along an r-axis with a zero polar angle.

Only two of the power schedules, 1a and 2a, have been used in the temperature-induced stress and displacement calculations for the full-scale experiments. Power schedules 1a and 2a were chosen because they give the highest temperature values, and hence the largest stresses and displacements, in group 1 and group 2, respectively.

4.1.1 Temperatures

The temperature calculations have been illustrated in the following two ways: as temperature profiles that show the time variation of the temperature rise and as contour plots that show the temperature distribution in space. Temperature profiles have been drawn for all six power schedules, assuming the infinite medium model. Contour plots have been made for power schedules 1a and 2a, and for both the infinite medium model and the isothermal boundary model in which the floor of the heater drift is idealized as a plane isothermal boundary. All the numerical values given are temperature rises rather than actual temperatures. However, in most of the cases considered, the temperatures are so high that the initial ambient rock temperature would be immaterial.

The profiles in Figs. 6a-6c [D6a,D6d,D6f] and Figs. 7a-7c [D7a, D7d,D7f] show the temperature rise in ^{o}C plotted against time (in days) for power schedules 1a, 2a and 2c. The temperature rise was evaluated for points lying along a radial vector formed by the intersection

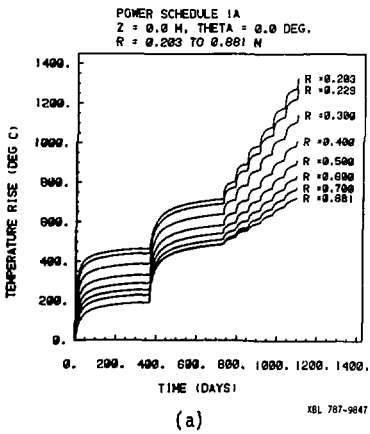

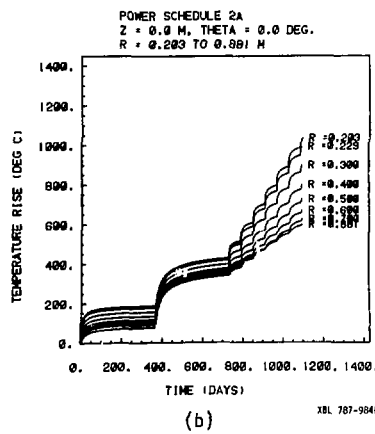

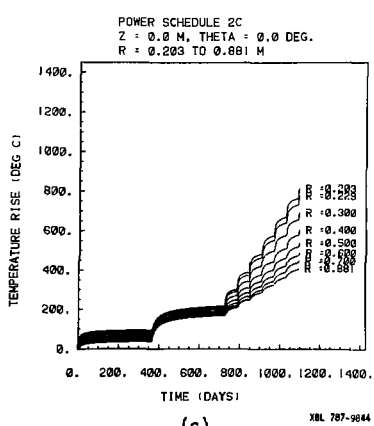

Figure 6 Temperature Profiles for Hanford Full-Scale Experiment: z = 0.0 m, θ = 0°, r = 0.203 to 0.881 m

of the heater midplane (z = 0) with the plane passing through the center line of the main heater and the center line of one of the peripheral heaters ($\theta = 0^{o}$).

Figures 6a-6c [D6a,D6d,D6f] give the temperature profiles for points falling within the ring of peripheral heaters (r = 0.203 to 0.881 m), and Figs. 7a-7c [D7a,D7d,D7f] give those for points falling outside of the ring of peripheral heaters ($r \geq 0.919$ m) to a distance of 5 m away from the central heater. Note that the vertical scale in Figs. 7a-7c [D7a,D7d,D7f] is exactly half that of Figs. 6a-6c [D6a,D6d,D6f]. Some significant values of r, whose temperature profiles have been plotted, are:

0.203 m = bore of 16-in. diameter central heater hole (initial design),

0.229 m = bore of 18-in. diameter central heater hole (updated design),

0.881 m = point at bore of peripheral heater hole closest to the central heater,

0.919 m = point at bore of peripheral heater hole farthest away from central heater.

Due to the low thermal conductivity of Pomona basalt (approximately half that of Stripa granite), exceedingly high temperatures will be reached. In the present calculations the thermal properties at 200°C (see Table 2 above) have been used. Since thermal conductivity of rocks (actually solids in general) decreases with temperature, even higher temperatures will be predicted if this dependence is taken into account.

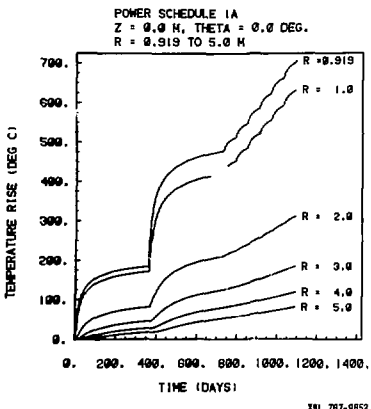

(a)

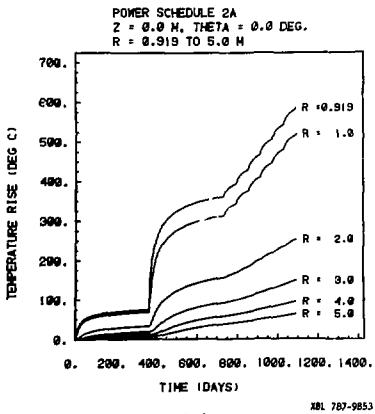

(b)

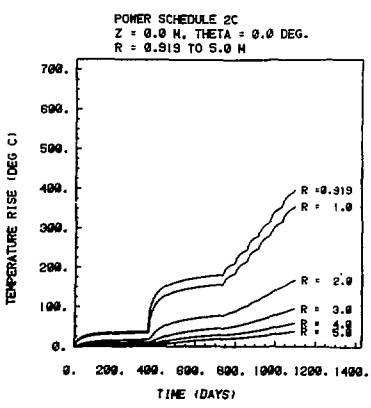

(c)

Figure 7 Temperature Profiles for Hanford Full-Scale Experiment: z = 0.0 M, θ = 0°, r = 0.919 to 5.0 m

Immediately after each power turn-on or power step-up event, the temperature increases very rapidly within the peripheral heater ring for 20 to 30 days. Thereafter the rise becomes more gradual until after 50 to 60 days, when the temperature changes so slowly that the heater-rock system can be said to be approaching a quasi-steady state. This shows that the 60-day duration between successive power steps is sufficient time for observation of the thermal effects due to a particular power step. Within a radius of 1 m from the central heater, distinct steps can be recognized on the temperature curves corresponding to successive power steps (Figs. 6a-6c [D6a,D6d,D6f]). Beyond 1 m the pulse nature of the power increase is attenuated by distance and the temperature rise follows smooth curves, Figs. 7a-7c [D7a,D7d,D7f]. Another important point to note is that the ring of 1-kW peripheral heaters increases the temperature within its circumference by 250°C. This represents a very extreme case of the ambient field.

Table 4 gives the temperature rise at the end of the first, second and third years of the experiment for selected values of r. Since it is probable that most of the instruments will be located 1 to 2.5 m from the central heater, the values of $r = 1$ and $r = 2$ have been included in Table 4. Maximum increases in rock temperatures at the end of the first, second, and third years have been predicted to be 440°C, 690°C, and 1270°C for the highest power considered (schedule 1a) and 85°C, 210°C, and 775°C for the lowest power (schedule 2c). Following the thermal guideline of Jenks (1977), where the zircaloy fuel cladding should not exceed 200°C, the initial power density of the spent fuel rod should not exceed 0.4 kW per meter at the time of burial, if

Table 4. Calculated temperature rise (°C) at the end of the first, second, and third years of the full-scale experiments.

		Temperature rise (°C) for different power schedules					
	Value of r(m)	1a	2b	1c	2a	2b	2c
First Year	0.229	440	430	220	175	170	85
	0.5	290	280	135	125	120	65
	1.0	170	163	88	70	65	35
	2.0	80	75	40	30	25	15
	5.0	25	12	7	5	5	2
Second Year	0.229	690	560	345	420	300	210
	0.5	535	420	265	360	235	180
	1.0	420	300	215	310	190	160
	2.0	210	150	100	155	90	75
	5.0	50	35	25	35	22	15
Third Year	0.229	1270	1140	915	1000	860	775
	0.5	885	755	615	695	575	405
	1.0	630	510	405	520	385	350
	2.0	312	240	190	250	185	165
	5.0	80	60	45	67	40	35

the spacing of spent fuel canisters is such that the interaction among them raises the ambient temperature by 100°C.

Table 5 contains the temperature rating of the instruments and the heater assembly, the incipient melting point of basalt, and the times at which those values will be reached for each power schedule and appropriate choice of radial distance from the central heater.

Although the heaters have been tested to 600°C in a mock-up test at LBL, it is reasonable to use a maximum rock temperature of 550°C as the temperature at which the heater may fail, to allow for the temperature difference due to radiative heat transfer across the air gap between the heater canister and the rock wall. From Table 5 and Fig. 6a, it can be seen that the central heater may fail in about 400 days after turn-on for power schedule 1a and in about 500 days for power schedule 1b. For all other power schedules, heater failure is expected to occur between two and three years, i.e., during the overload test.

The extensometers and stressmeters (USBM or IRAD gauges) are designed to function properly up to temperatures of 200°-250°C. Beyond these temperatures the instruments would "fail" either because of component failure or because the methods of calibration or data reduction are no longer valid. According to the thermal calculations, Tables 4 and 5, extensometers and stressmeters placed inside the ring of peripheral heaters may fail before the end of the first year for power schedules 1a, 1b, and 1c and during the second year for power schedules 2a and 2b. All extensometers and stressmeters at radial distances between 1 m and 2 m from the central heater are expected to fail before 640 days

Table 5. Significant temperature values and predicted times at which the temperature is attained for an infinite medium model.

Temperature (°C)	Significance	Value of r (m)	Time (days) temperature value is reached at designated value of r for different power schedules					
			1A	1B	1C	2A	2B	2C
100°	Boiling point of water	0.229	1.2	4	4	7	181	371
200°-250°	Estimated temperature rating of instruments†	0.5	60-90	190-215	395-415	380-400	420-735	740-800
		1.0	360-375	375-415	560-819	390-435	735-835	805-900
		2.0	640-890	945-*	1095-*	900-1075	*	*
500°-600°C	Estimated temperature rating of heater assembly	0.229	385-420	395-740	815-910	760-860	860-920	910-980
1050°	Incipient melting point of basalt‡	0.229	980	1085	*	*	*	*

*Temperature is not reached within the three-year test period.

†This includes extensometers, IRAD and USBM gauges.

‡Ekren, et al., 1974, see also Presnall, et al., 1972.

for power schedule 1a. For other power schedules, some of these instruments will survive the two-year test period before the overload test.

During the overload test, i.e., in the third year of the full-scale experiments when the power of the central heater is stepped up by 1 kW every 60 days, heater failure is likely to occur for all of the power schedules. If the heater assembly continues to function at temperatures above 600°C, the temperature at the edge of the heater hole will increase beyond 1050°C, the incipient melting point of basalt (Ekren et al., 1974; Presnall et al., 1972), for power schedules 1a, 1b, and 2a.

For all power schedules except the two lowest, 2b and 2c, all extensometers and stressmeters placed within a radius of 2 m from the central heater are susceptible to failure as the temperatures exceed 250°C during the third year of the experiment.

It is evident from Table 5 that some of the temperatures predicted for the later stages of the full-scale experiments are hypothetical. A number of drastic events such as heater failure, thermal run-away resulting from borehole decrepitation or rock melting would have happened, invalidating the present calculations.

The values given in Tables 4 and 5 pertain to the infinite medium model and therefore, represent conservative (slightly high) estimates of temperatures. The correct temperatures should lie somewhere between those obtained from the infinite medium and isothermal boundary condition models as demonstrated numerically by Chan et al. (1978).

Contour plots showing the temperature distribution in a vertical half-plane have been made for both of the models previously described for power schedules 1a and 2a. (Power schedule 1a is designated by "MAIN HTR = 5 kW," and power schedule 2A is designated by "MAIN HTR = 2 kW.") The following combinations of power schedule with model have been included in the text:

Figs. 8a,8b [D8e,D8i]
- power schedule 1a, infinite medium model;

Figs. 9a-9c [D9b,D9e,D9i]
- power schedule 2a, infinite medium model;

Figs. 10a, 10b [D10e, D10i]
- power schedule 2a, infinite medium model;

Figs. 11a-11c [D11b,D11e,D11i]
- power schedule 2a, isothermal boundary model.

Appendix D contains a time series of contour plots for each of the four categories above. Each contour plot shows the temperature distribution in a vertical half-plane passing through the centers of the central heater and one peripheral heater and bounded on the left by the z-axis. The section of the z-axis shown extends from 8 m below the heater midplane to 4.25 m above it, which is the assumed location of the floor of the heater drift. The highest isotherm was chosen to be the value of the temperature rise at the edge of the central heater hole on the midplane ($r = 0.229$ m, $z = 0$ m, $\theta = 0^{o}$). Contour levels of 100^{o}, 75^{o}, 50^{o}, 25^{o}, and 5^{o} are shown on every graph. Contour values larger than those are usually at 50^{o} or 100^{o} intervals.

The effect of the assumed boundary condition first becomes apparent on day 30 (Figs. 9a [D9b], 11a [D11b]). The 5^{o} isotherm is no longer symmetric with respect to the heater midplane in the isothermal boundary

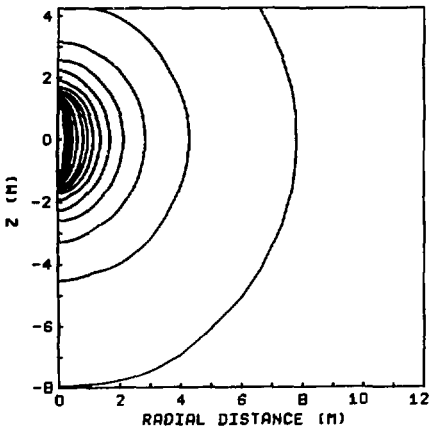

XBL 787-9501

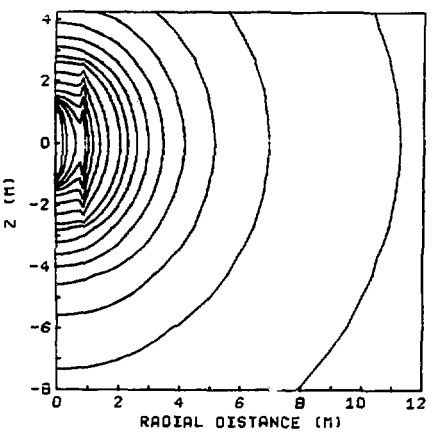

XBL 787-9507

Figure 8 Isotherms in Vertical Plane, Hanford Full-Scale Experiment: Infinite Medium Model, Main Heater = 5 kW

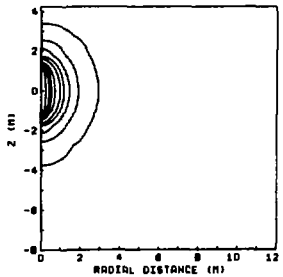

PLOT INFORMATION

TIME = 30. DAYS

THETA = 0.0 DEG.

ISOTHERMAL BOUNDARY MODEL

MAIN HTR = 5.00 KW
PERIPHERAL HTR = 1.00 KW

CONTOURS (DEG.C.) PLOTTED -
360. 260. 200. 160.
100. 75. 50. 25.
5.

(a)

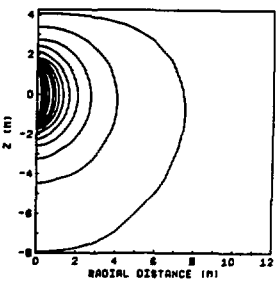

PLOT INFORMATION

TIME = 365. DAYS

THETA = 0.0 DEG.

ISOTHERMAL BOUNDARY MODEL

MAIN HTR = 5.00 KW
PERIPHERAL HTR = 1.00 KW

CONTOURS (DEG.C.) PLOTTED -
440. 400. 350. 300.
250. 200. 175. 150.
125. 100. 75. 50.
25. 5.

(b)

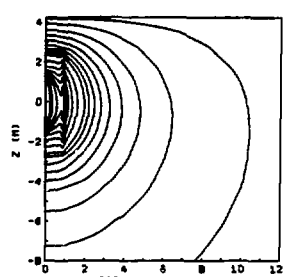

PLOT INFORMATION

TIME = 730. DAYS

THETA = 0.0 DEG.

ISOTHERMAL BOUNDARY MODEL

MAIN HTR = 5.00 KW
PERIPHERAL HTR = 1.00 KW

CONTOURS (DEG.C.) PLOTTED -
677. 600. 500. 450.
400. 350. 300. 250.
200. 175. 150. 125.
100. 75. 50. 25.
5.

(c)

Figure 9 Isotherms in Vertical Plane, Hanford Full-Scale Experiment: Isothermal Boundary Model, Main Heater = 5 kW

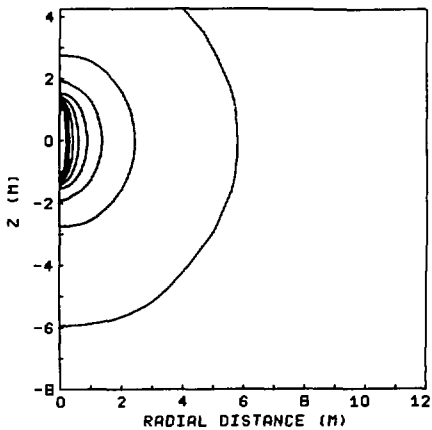

XBL 787-9461

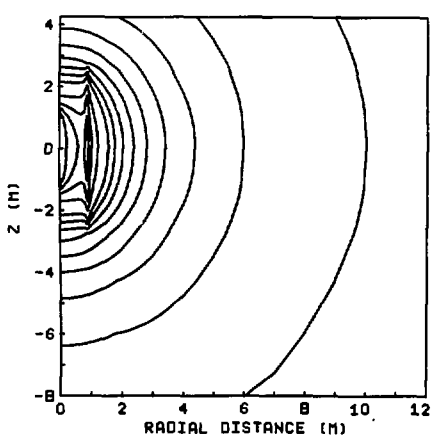

XBL 787-9460

Figure 10 Isotherms in Vertical Plane, Hanford Full-Scale Experiment: Infinite Medium Model, 2-kW Main Heater

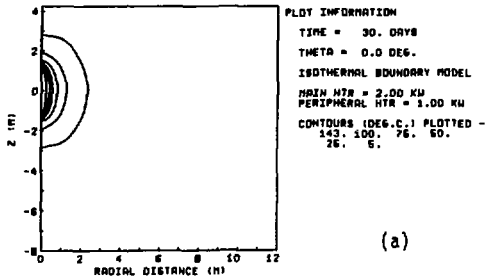

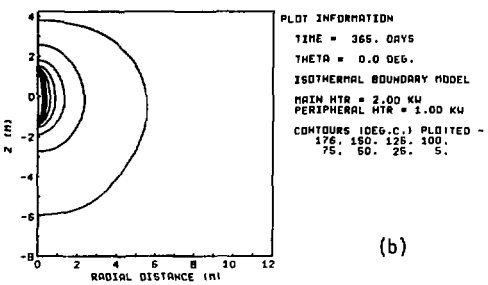

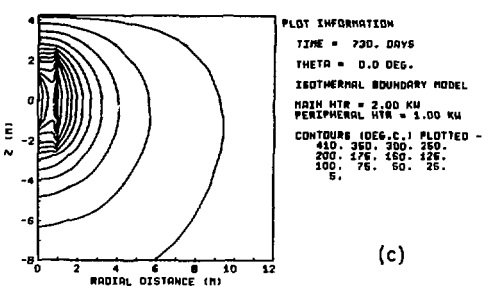

Figure 11 Isotherms in Vertical Plane, Hanford Full-Scale Experiment: Isothermal Boundary Model, 2-kW Main Heater

model. This difference becomes more prominent with time as heat diffuses toward the boundary. It is also interesting to note that within a half-meter radius of the central heater, there is very little variation in temperature with vertical distance over the length of the heater. However, a vertical thermal gradient always exists above and below the heater.

Because of the low thermal diffusivity of Pomona basalt, the isotherms have moved out radially from the 5-kW central heater by only 2 m during the first year (Figs. 8a [D8e], 9b [D9e]), and by an additional 1.5 m during the second year (Fig. 8b [D8i], 9c [D9i]). The migration away from the 2-kW central heater is even slower, approximately 0.5 m during the first year (Figs. 10a [D10e], 11a [D11e]), and another 1.25 m during the second year (Fig. 10b [D10i], 11b [D11i]).

4.1.2 Displacements

The displacement results are represented by three types of plots: deformation of the heater drift and borehole, vertical displacement (u_z) plotted against z, and radial displacement (u_r) plotted against r. The combination of models with power schedules has been summarized in Table 3.

Figures 12a [D12a] and 12b [D12b] show the expected deformation of the heater drift and heater borehole at the end of the second and third years of the experiment for power schedule 1a. The outline of the heater drift and borehole has been indicated by a solid line (see also the finite element mesh shown in Fig. 5b [D5b]). The symbols designated "Mesh 1" represent the deformed shape of an imaginary boundary in an infinite rock medium and those symbols designated "Mesh 7" represent

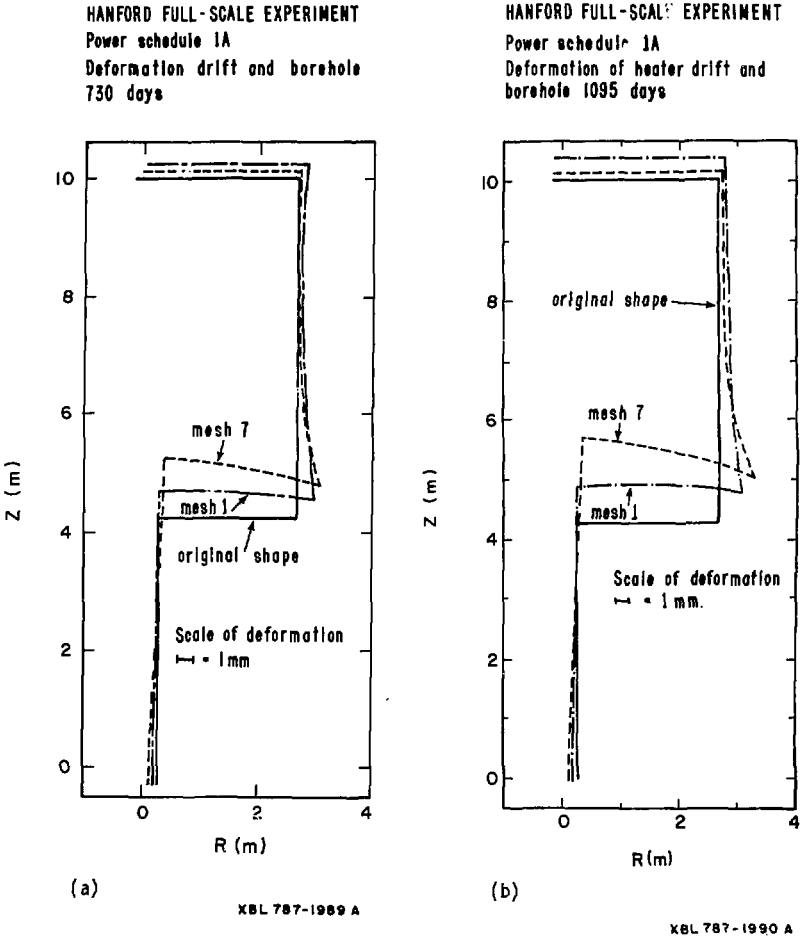

Figure 12 Deformation of Heater Drift and Borehole under Power Schedule 1a, Hanford Full-Scale Experiment

the deformed periphery of the heater drift, which is tilted by the thermal loading. Note the greatly exaggerated scale used to display the deformation. The deformed shape resembles that presented in a previous study for a Canadian repository (Chan, 1979).

The largest vertical displacements occur, for both Mesh 1 and Mesh 7, along the center line of the floor of the drift. However, the magnitude of the displacement for the Mesh 7 results are almost twice those for Mesh 1 because of the absence of rock in the drift in Mesh 7; the maximum values for each case studied have been listed in Table 6. These displacements, representing average strains on the order of 10^{-3} over a few meters, are very substantial for a crystalline rock. Measurement of the convergence between the floor and the roof of the heater drift should provide valuable data for repository design and experience for monitoring during the operating period. However, since the experiments are to be started up shortly after the completion of the excavation, part of the convergence observed may be due to the time-dependent response of a jointed rock mass to excavation stress. It is, therefore, necessary to install convergence meters (extensometers) at two or more locations, including one very close to the center line of one of the full-scale experiments and one as far away as possible so that the excavation-induced and thermally induced displacements can be unraveled.

Vertical displacements have been plotted at three different radial distances from the central heater. The three radii chosen are: inside the ring of the peripheral heaters, at r = 0.45 m (Fig. 13a [D17a]); at a distance of almost one meter from the ring of peripheral heaters,

Table 6. Maximum predicted vertical displacement, u_z, 0.375 m below the floor of the heater drift (full-scale experiments), Mesh 1 and Mesh 7.

Time (days)	Maximum Value of u_z (mm)			
	Power Schedule 1a		Power Schedule 2a	
	Mesh 1	Mesh 7	Mesh 1	Mesh 7
730	2.0	4.2	1.5	3.2
1095	2.8	6.2	2.4	5.0

at r = 1.875 m (Fig. 13b [D18a]); and midway between the two full-scale experiments, at 10.5 m from each central heater (Fig. 13c [D19a]). Results for both Mesh 1 and Mesh 7 and power schedules 1a and 2a have been included in Appendix D; the only times represented are before and after the overload test, at 730 and 1095 days.

Two trends illustrated by Figs. 13a [D17a], 13b [D18a], and 13c [D19a] are that (i) the maximum value of the magnitude of the vertical displacement decreases with distance away from the central heater, and that (ii) the peak of the u_z - z curve occurs farther away from the heater midplane, as the distance from the central heater increases. Table 7 lists the maximum displacement for each case covered mentioned above. Note also that the values for Mesh 7 are approximately 80% larger than those for Mesh 1 at r = 0.45, 1.875 m and nearly equal to those for Mesh 1 at r = 10.5 m.

The vertical displacements at the midpoint between the two full-scale experiments are small, less than half a millimeter in every case except one, but the interference between displacements of the two full-scale experiments, one with power schedule 1a and the other with 2a is significant (Fig. 13a [D19a]). At the end of two years, the maximum superimposed value of u_z midway between the two experiments is 0.65 mm for Mesh 7 (Fig. 13c [D19a]) and after the overload testing, the value is 1.25 mm, also for Mesh 7. These values are approximately 20% of the maximum vertical displacements closer to the hotter experiment (power schedule 1a). The corresponding values for Mesh 1 are slightly smaller than those for Mesh 7. Near the heaters, however, the differences between the calculated displacements for the two meshes

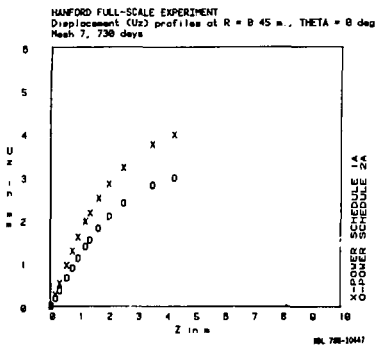

(a)

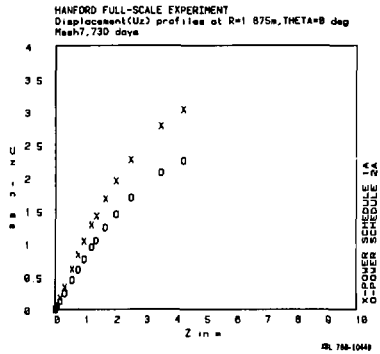

(b)

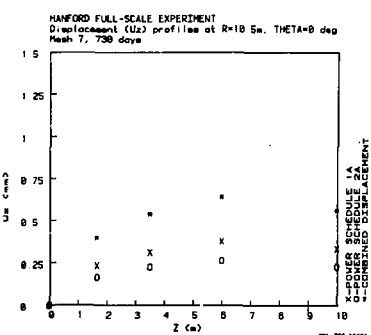

(c)

Figure 13 Displacement Profiles (u_z) for Mesh 7, 730 days, Hanford Full-Scale Experiment

Table 7. Maximum predicted vertical displacements (u_z) at various radial distances (full-scale experiments), $\theta = 0^{\circ}$.

Power Schedules	Mesh 1			Mesh 7		
	Radial distance (m)*					
	0.45	1.875	10.5	0.45	1.875	10.5
	730 DAYS					
1a						
max u_z (mm)	2.10	1.68	0.38	3.9	3.0	0.38
value of z (m) at which max occurs	3.85	3.70	7.5	†	†	6.5
2a						
maximum value of u_z (mm)	1.55	1.24	0.24	2.9	2.2	0.26
value of z (m) at which max occurs	3.85	3.55	7.5	†	†	6.5
Combined						
maximum value of u_z (mm)	-	-	0.62	-	-	0.64
value of z (m) at which max occurs	-	-	7.5	-	-	6.5
	1095 DAYS					
1a						
maximum value of u_z (mm)	3.10	2.48	0.63	5.8	4.3	0.62
value of z (m) at which max occurs	2.65	3.60	8.0	†	†	7.5
2a						
maximum value of u_z (mm)	2.55	2.02	0.49	4.7	3.6	0.48
value of z(m) at which max occurs	2.65	3.50	8.0	†	†	7.5
Combined						
maximum value of u_z (mm)	-	-	1.10	-	-	1.1
value of z(m) at which max occurs	-	-	8.0	-	-	7.5

*Radial distance from the center line of the central heater of the respective experiment. The only point at which the vertical displacements have been superimposed is midway between the two full-scale experiments (assuming that the two full-scale experiments are separated by 21 meters).

†Maximum displacement occurs at the floor of the heater drift, z = 4.25 m.

are much greater. Table 7 lists the maximum displacement for each power schedule. The general trends described in the preceding paragraph are again evident.

Figures 14a-14f [D20b-D20f,D20i] show u_r plotted against r for points in the heater midplane at selected times, for the Mesh 1 calculations only. Appendix D contains a more complete time series of these plots made to correspond to those times at which the series of contour plots (also in Appendix D) were made. This series of plots clearly illustrates how the shape of the u_r-r curve changes. Over time, the peak of the displacement curve moves farther away from the central heater and the temperature field spreads over a larger region (Figs. 14a [D20b], 14b [D20c], 14c [D20d], 14d [D20e]), until the peripheral heaters are energized. The effect of the peripheral heaters is to sharpen the peak of the curve (Fig. 14e [D20f]) and decrease the distance between the peak and the central heater. Stepping up the power of the central heater has an effect similar to that of the peripheral heaters. Note that the wall of the heater hole moves inward at all times as a result of the combined effect of thermal loading and confinement. The maximum values of u_r and the values of r at which they occur are listed in Table 8.

In addition, plots for Mesh 7 were made at two times, at the end of the second and third years of the experiment, though only the former has been included in the text. In contrast to that for Mesh 1 (Fig. 14f [D20i]), the shape of the displacement profile for Mesh 7 (Fig. 15 [D22a]) is quite flat between r = 2 m and 10 m, showing the influence of the extensometer drift. Therefore, the presence of the

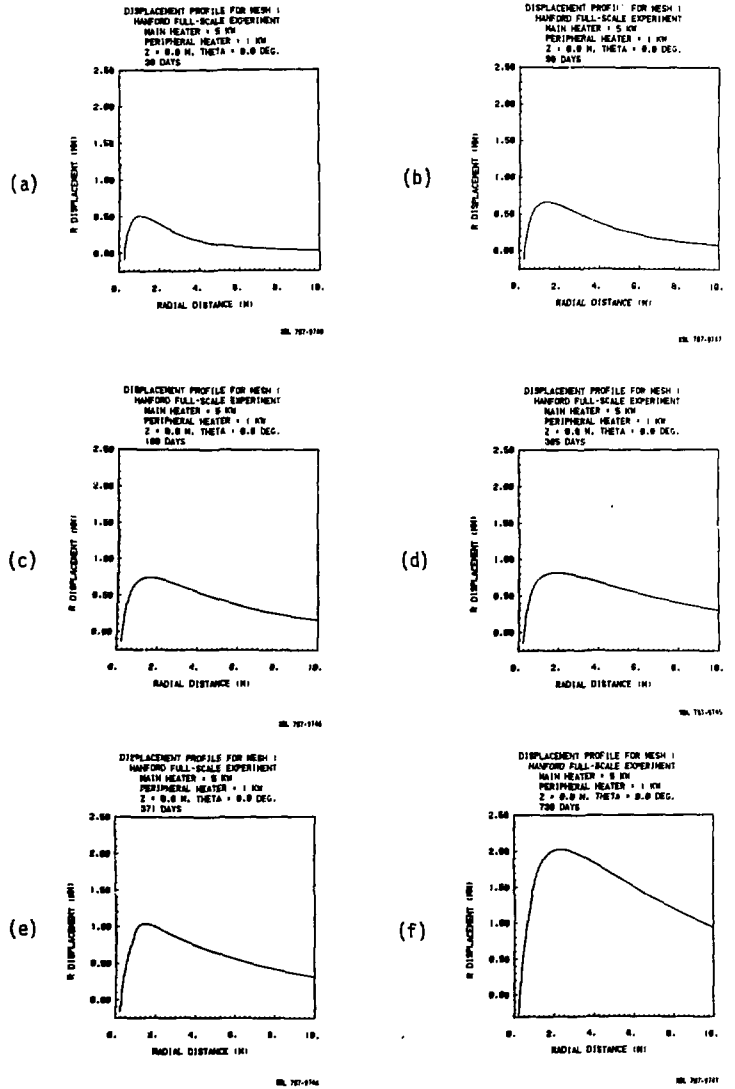

Figure 14 Displacement Profile (u_r) for Mesh 1, Hanford Full-Scale Experiment. Main Heater = 5 kW; $z = 0.0$ m; $\theta = 0^0$

Table 8. Maximum predicted radial displacement, u_z, in the midplane (full-scale experiments).

Time (days)	Power schedule 1a: Max u_r (mm)	Power schedule 1a: Value of r(m) at which max u_r occurs	Power schedule 2a: Max u_r (mm)	Power schedule 2a: Value of r(m) at which Max u_r occurs
MESH 1				
7	0.27	0.75	0.11	0.75
30	0.50	1.2	0.20	1.1
90	0.66	1.5	0.27	1.4
180	0.75	1.7	0.30	1.55
365	0.82	1.9	0.35	1.90
371	1.04	1.5	0.55	1.40
390	1.35	1.5	0.85	1.6
450	1.68	2.0	1.15	1.9
730	2.04	2.3	1.50	2.5
760	2.10	2.35	1.58	2.3
790	2.15	2.4	1.64	2.4
1095	3.00	2.2	2.48	2.2
MESH 7				
730	1.91	2.5	1.41	2.60
1095	2.90	2.25	2.35	2.30

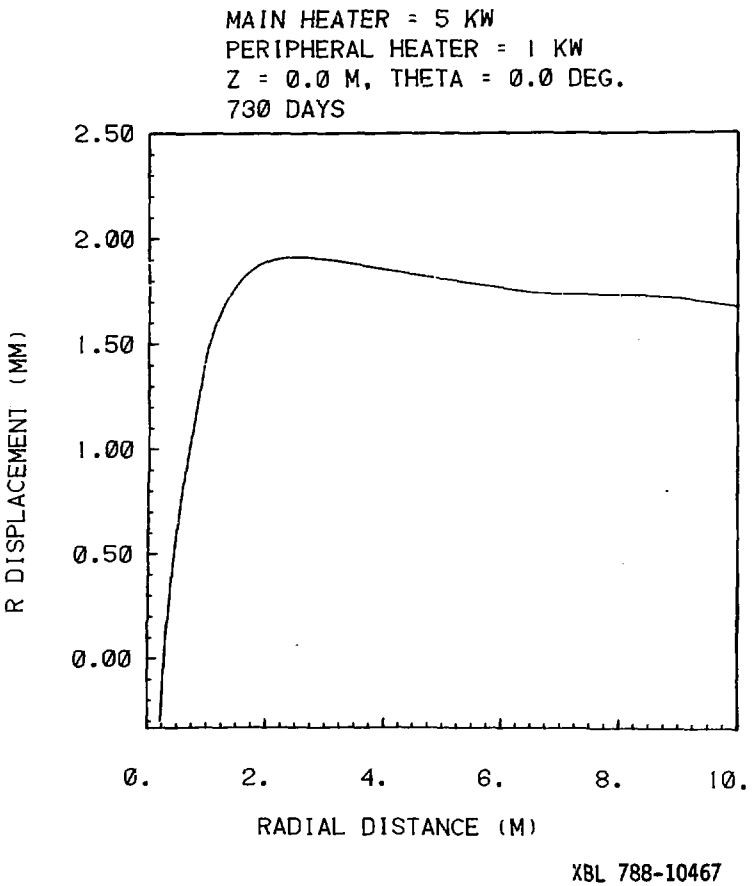

Figure 15 Displacement Profile (u_r) for Mesh 7, Hanford Full-Scale Experiment. Main Heater = 5 kW; z = 0.0 m, $\theta = 0^{o}$; 730 days.

extensometer drift should be taken into account both in the placement of anchor points and the interpretation of the results. During the later stages of the experiment, little relative displacement is to be expected between an anchor point lying in the range $2 \leq r \leq 10$ m and the head of a horizontal extensometer.

The remarkable effect of the extensometer drift demonstrated in Figs. 14f [D20i] and 15 [D22a] occurs only at later times. At the beginning of the experiment the difference between the two models (i.e., with or without the drifts) is smaller (not illustrated). Also, the effect predicted by the axisymmetric model applies only to the horizontal extensometers at right angles to the extensometer drift. For extensometers at an inclined angle, the effect of the free surface is expected to be less serious.

A discussion of the interference of the radial displacements due to the two full-scale experiments is given in subsection 4.1.4 below.

4.1.3 Stresses

The stress plots fall into two categories: those made along a radial vector lying in the heater midplane and those made along the floor of the excavation tunnel. The plots of the results in the first category show the three components of stress, σ_r, σ_θ, σ_z, (designated S_R, S_θ, and S_z in the plots), plotted against radial distance. Calculations were made for power schedules 1a and 2a for Mesh 1, but only results for power schedule 1a have been included in the text. (The complete set of stress plots in Appendix D, Volume 2, form a time series and also include results for power schedule 2a.)

The following generalizations can be made from these graphs. The compressive (positive) stress increases in time (note that the scale along the ordinate varies from graph to graph) but with the exception of σ_r which has a peak, decreases with distance from the central heater. As time passes the tensile (negative) stress decreases but is spread out over a longer distance (Figs. 16a-16c [D24a-D24c]). In addition, there is little change in the shape of the curves until the peripheral heaters are turned on. The only exception to this is that the gradient of the σ_θ and σ_z curves near the central heater decreases in time as a result of the corresponding decrease in the thermal gradient. The effect of energizing the peripheral heaters is seen as a sharp peak at r = 0.9 m on the σ_θ and σ_z curves and as a decrease in the gradient of the σ_r curve to the right of its maximum (Figs. 16d, 16e [D24f,D24g]).

It is important to note that the predicted stress values are quite high, even for early times in the experiment. Table 9 gives the maximum values of each stress component for the times plotted. If the rock mass behaves as a continuum with elastic properties similar to those measured in laboratory specimens, then it is likely that hole decrepitation will occur. The value of stress at which underground rock fails is uncertain, but is believed to be much lower than measurements made in the laboratory. Laboratory measurements on the compressive strength of Pomona basalt have yielded a range of 75-378 MPa depending on the confining pressure (Duvall et al., 1978). For decrepitation of the heater hole, the unconfined compressive strength

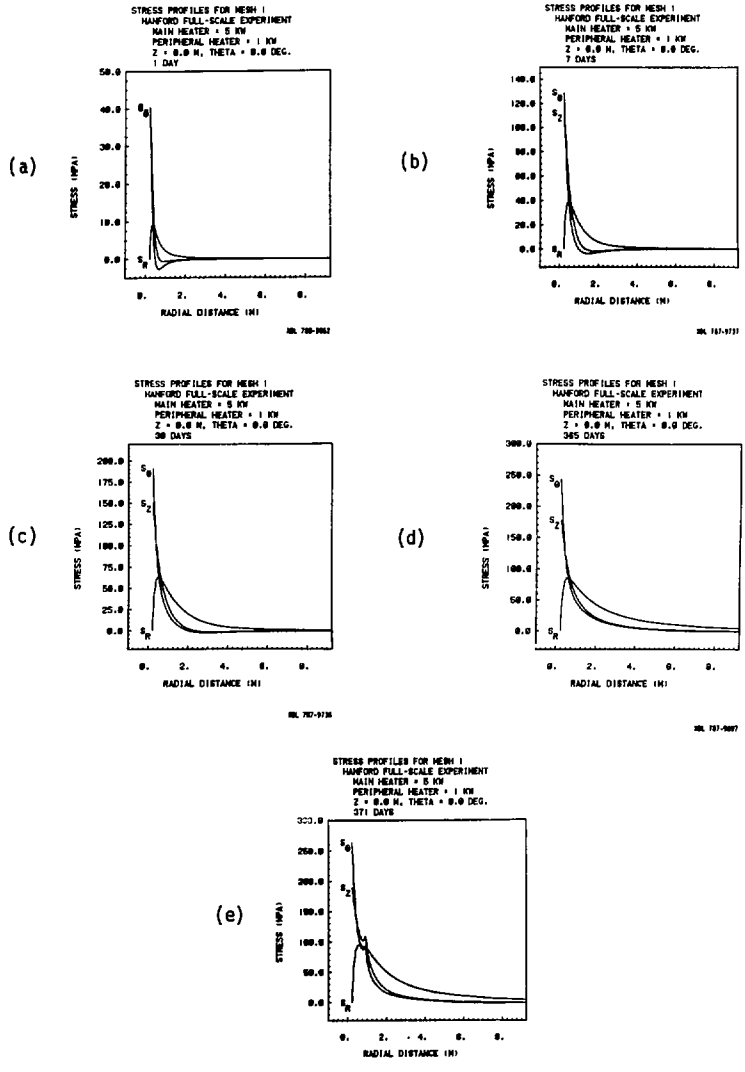

Figure 16 Stress Profiles for Mesh 1, Hanford Full-Scale Experiment. Main Heater = 5 kW; z = 0.0 m, $\theta = 0^{0}$

Table 9. Maximum predicted compressive stresses in the heater midplane (full-scale experiments) for Mesh 1 ($\theta = 0^{o}$).

	Power Schedule 1a			Power Schedule 2a		
Time (days)	max σ_r*	max σ_θ†	max σ_2†	max σ_r*	max σ_θ†	max σ_2†
1	9.2	40.3	40.6	3.7	16.1	16.2
7	38.0	129.3	112.4	15.2	51.7	45.0
30	63.0	191.9	150.1	25.2	76.7	60.0
90	75.7	222.5	166.7	30.2	89.0	66.7
180	81.0	235.4	173.5	32.4	94.1	69.4
365	85.1	244.8	178.4	34.0	97.9	71.4
371	94.9	264.2 93.4	189.7 109.4	43.9	117.2 61.4	82.6 71.8
390	115.7	312.2 114.3	221.4 134.7	66.1	164.9 82.1	114.2 96.8
450	136.0	358.1 137.6	247.6 158.6	87.3	209.9 104.9	139.9 120.4
730	154.4	397.4 159.0	268.4 179.2	105.2	246.6 125.0	159.4 139.6
760	166.8	437.4 165.1	299.3 187.3	115.7	286.4 130.9	190.1 147.5
790	169.4	443.1 168.0	302.3 190.1	118.3	291.9 133.7	193.1 150.3
1095	261.8	714.3 -	502.8 -	208.2	561.7 -	392.9 -

*Maximum value occurs between 0.4 and 0.9 m.

†Maximum value occurs at edge of heater hole, r = 0.229 m; where two values are given, second value is local maximum near r = 0.9 m.

should apply. According to Table 9, these values will be reached before the overload testing begins.

The second set of plots show σ_θ and σ_r plotted for points along the floor of the heater drift. (Actually the values are for points located 0.375 m beneath the floor of the heater drift at z = 3.875 m.) Plots were made for power schedules 1a and 2a, for Mesh 7 only. Figures for 730 days have been included in the text; Appendix D contains results for both 730 and 1095 days.

Both the tangential and radial stresses are tensile over a large region around the heater hole along the floor of the heater drift, Fig. 17 and Fig. 18. The value of r at which σ_θ becomes compressive is approximately 2.8 m (Fig. 17 [D26a]) and the value for σ_r is 1.75 m (Fig. 18 [D27a]) at the end of two years. The tangential stress (Fig. 17 [D26a]) increases quite rapidly with r near the central heater and then more slowly until r = 0.5 m is reached. After that the slope of the curves is again quite steep and at r = 3.25 m a sudden drop occurs, corresponding to the location of the wall of the heater drift. The curve falls slowly after that.

The radial stress (Fig. 18 [D27a]), in contrast, decreases between the central heater and ring of peripheral heaters. A slight kink in the curves indicates the location of the peripheral heaters. Outside the ring of peripheral heaters the curve increases quickly until a sudden drop occurs at r = 3.25 m, as explained above.

Table 10 contains the maximum values of the tensile stress at the end of two and three years. These values, σ_θ in particular, are extremely high, exceeding the mean tensile strength of intact Pomona

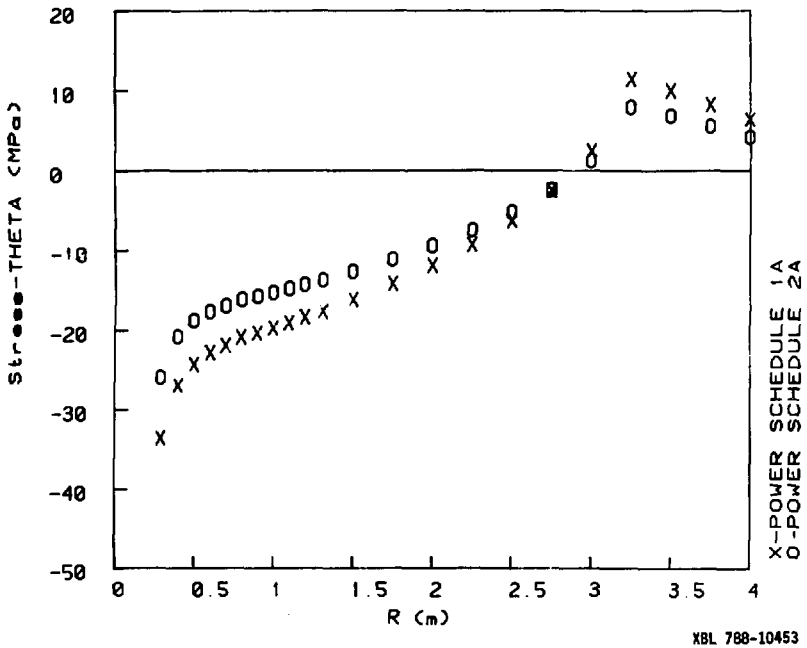

Figure 17 *Tangential Stress Along Floor of Heater Drift* (z = 3.875 m), Hanford Full-Scale Experiment. Mesh 7, 730 days

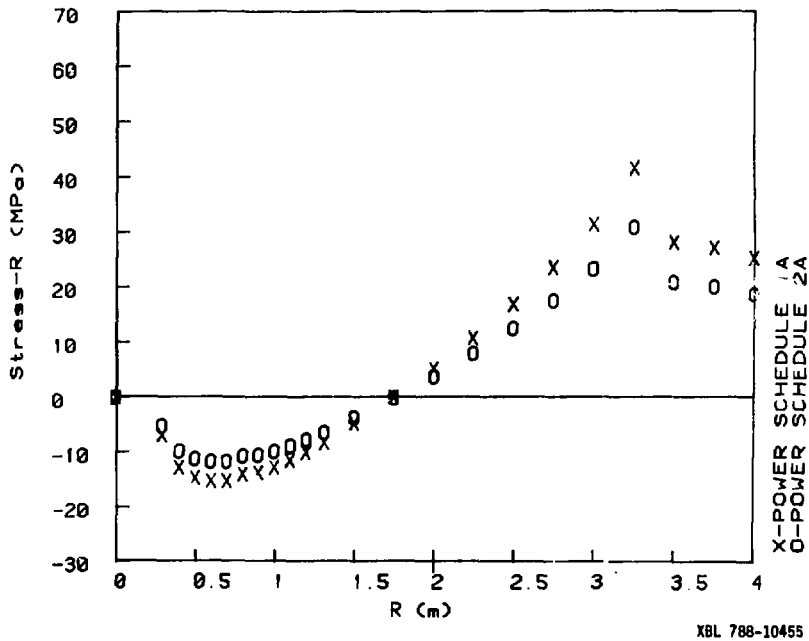

Figure 18 Radial Stress Along Floor of Heater Drift (z = 3.875 m), Hanford Full-Scale Experiment. Mesh 7, 730 days

Table 10. Maximum predicted stress 0.375 m below the floor of the heater drift (full-scale experiment), Mesh 7.

	σ_θ (MPa)			
	Maximum Tensile*		Maximum Compressive	
	Power Schedule			
Time (days)	1a	2a	1a	2a
730	34	27	12	8
1095	48	42	18	14
	σ_r (MPa)			
730	16	15	42	32
1095	23	20	62	50

*These values are the maximum absolute value of the tensile stress.

basalt given by Duvall et al. (1978). According to a recent hydrofracture measurement by Haimson (1978), the horizontal components of the virgin state of stress in the Near Surface Test Facility horizon are approximately 0.7 MPa and 7-14 MPa in the directions normal and parallel to the length of the ridge. The net tensile stress will thus exceed the tensile strength some time during the experiment in both cases given in Table 10, and cracking of the drift floor is likely to occur if the rock is responding as a linear elastic continuum.

The stress values in Table 10, however, may have been overestimated, because the temperatures from the infinite medium model have been used as the thermal load. To check this, the thermomechanical calculations should be repeated using temperatures calculated by a numerical method which models the heater drift with the proper convective boundary conditions.

In addition, the very small horizontal in situ stress in one direction cast some doubt on the validity of an axisymmetric model with a fixed displacement boundary condition. A first step in checking the validity of the displacement boundary condition would be to repeat the stress calculation by applying the minimum in situ horizontal stress to the outer boundary of the axisymmetric model and compare the results with the fixed boundary model. If the results agree, then the axisymmetric model with fixed displacement boundary condition can still be applied. The total resultant stress can be obtained by superposition if the rock is assumed to be a linear elastic continuum.

In the present preliminary calculations the rock mass has been treated as a continuum as a first approximation. In reality numerous discontinuities of various sizes and spacings exist in the rock mass (Goodman, 1976). The closely spaced discontinuities can be treated by an equivalent medium approach in which the rock mass is modeled as an anisotropic continuum with reduced elastic moduli. The larger discontinuities have to be modeled individually (Goodman et al., 1968; Noorishad et al., 1971; Gale et al., 1974; Ayatollahi, 1978; Ayatollahi et al., 1979). In view of the lower elastic moduli and possibly lower thermal expansion coefficient expected in a fractured rock mass, the thermal stress and displacement would be lower than those predicted here using a continuum model. This has been found to be the case during the Stripa experiments (Cook and Hood, 1978). In particular, tensile stresses may or may not be transmitted across discontinuities, depending on the nature of the filling material. On the other hand, the in situ compressive and tensile strengths may also be substantially below the intact rock values, and therefore both compressive and tensile failure may still occur with consequent lowering of thermal conductivity and enhancement of permeability. It is necessary to measure the elastic moduli, the joint stiffness and thermal expansion coefficient and their temperature and time dependence in situ and/or in large blocks of rock containing discontinuities in order to provide realistic input parameters for proper nonlinear numerical modeling.

4.1.4 Interference between the two full-scale experiments

An investigation of the possible interference of one full-scale experiment with the other is necessary to design the experiment and

to determine the ultimate spacing of the waste canisters in a rock repository. To this end, we superimposed the temperature, stress, and displacement profiles of the two full-scale experiments. A separation of 21 m was used between the central heaters of the two experiments. In the figures, the experiment on the left follows power schedule 1a and the one on the right follows schedule 2a. Calculations were made along the midplane for Mesh 1. Here, only the plots showing the maximum degree of interference, corresponding to 730 and 1095 days, are included. On the basis of earlier remarks on the large temperature and stress values, the values plotted may be largely hypothetical.

The interference of the temperature fields for the two experiments is hardly significant when compared to the large temperature values near the heaters. At the midpoint between the two experiments, $r = 10.5$ m, the combined temperature rise is about 10°C for 730 days (Fig. 19 [D28a]) and about 20°C for 1095 days, less than 2% of the peak temperature due to the higher power experiment.

By contrast, a barely overlapping temperature distribution does not imply an insignificant stress or displacement value at the midpoint. Compressive stress is additive and the value of σ_r at 10.5 m is 18 MPa for 730 days (Fig. 20 [D29a]) and 25 MPa for 1095 days. These values are approximately 10% of the maximum values shown on each graph.

The most significant influence of one experiment on the other can be seen in the plots of radial displacement (Fig. 21 [D30a]). The direction of positive displacement has been chosen as the direction from the 5-kW central heater (power schedule 1a) on the right to the 2-kW central heater (power schedule 2a) on the left. This means that

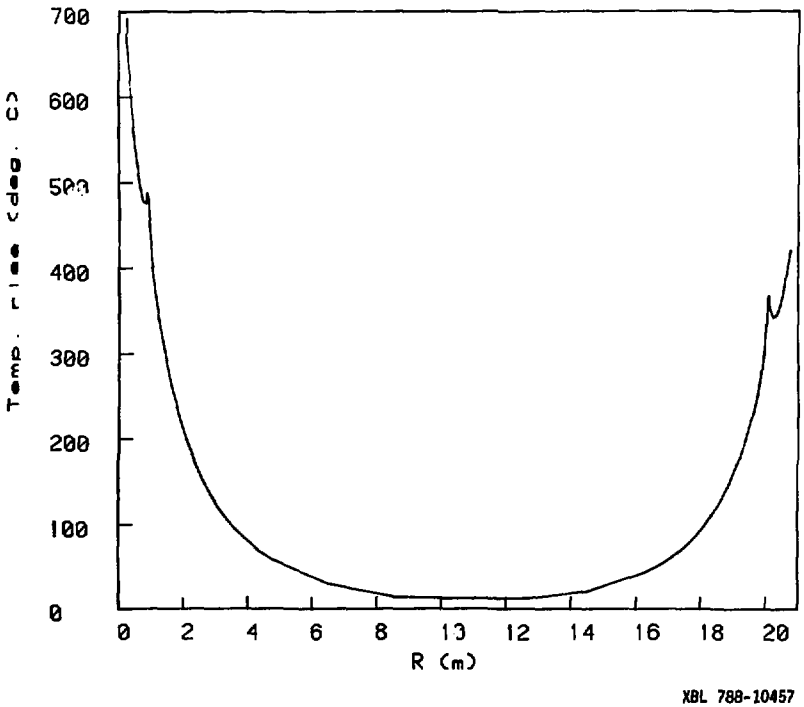

Figure 19 Interference Between the Two Full-Scale Experiments: Combined Temperature Profile at z = 0 m, θ = 0°; Infinite Medium Model; 730 days

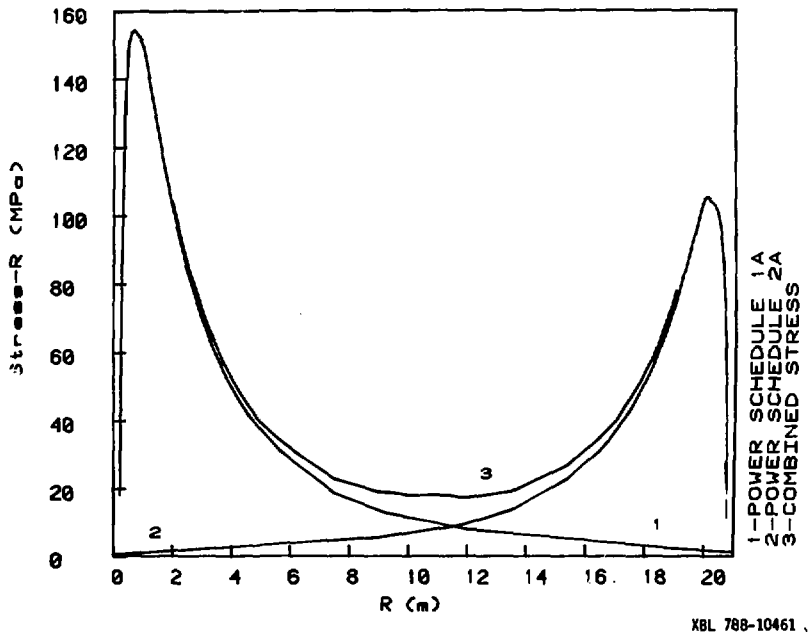

Figure 20 Interference Between the Full-Scale Experiments: Stress (σ_r) Profiles at z = 0 m, $\theta = 0^0$; Mesh 1, 730 days

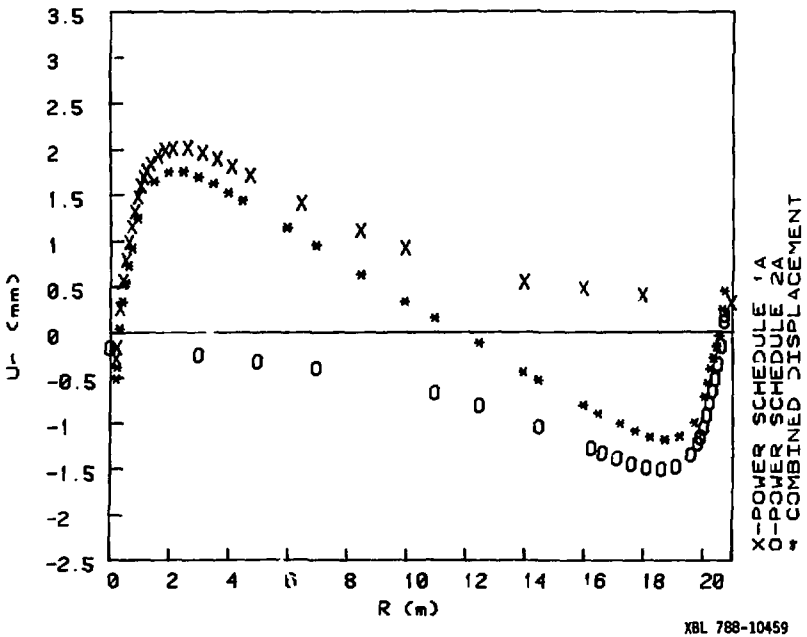

Figure 21 Interference Between the Two Full-Scale Experiments: Displacements (u_r) Profiles at z = 0 m, $\theta = 0^{\circ}$; Mesh 1, 730 days

the displacements must be combined according to their signs. The interference between the two experiments reduces the radial displacement which would occur if only one full-scale experiment were operating. In fact, the radial displacements of the two full-scale experiments cancel one another at r = 12 m, whereas the value for each individual experiment would be close to 40% of the individual maximum u_r (Fig. 21 [D30a]). Even near each central heater, the effect of the other experiment is not negligible, as can be seen from Table 11, which gives the changes in radial displacement caused by the influence of one full-scale experiment on the other for several values of r. Here the interference between the two experiments has been evaluated along a common radius and, therefore, represents the maximum possible. Since the horizontal extensometer will be either normal to or inclined at an angle to this line, the measured interference is expected to be less.

The plots which show the combined vertical displacements were discussed in an earlier section.

An important point to emerge is that although the high temperature zone is quite localized, the thermally induced displacement, being a cumulative effect, is significant over a much larger region. This is also true of the thermal stress, though to a lesser extent. In the interpretation of the field data, comparison should be made with the superimposed predicted displacements and stresses, lest the experimental results may be misunderstood as due to anisotropy of the rock mass. In deciding on the separation between adjacent storage rooms

Table 11. Predicted combined radial displacements in heater midplane of the two full-scale experiments, Mesh 1.

	u_r (mm), 730 days, for the following values of r(m)*					
	2.5	5.0	10.5	12.0	16.0	18.5
Power Schedule 1a	2.00	1.65	0.85	0.75	0.45	0.30
Power Schedule 2a	-0.25	-0.35	-0.60	-0.75	-1.25	-1.50
Combined	1.75	1.30	0.25	0.00	0.80	-1.20
Fractional Change†	0.13	0.21	0.71	1.0	0.36	0.2
	u_r (mm), 1095 days, for the following values of r(m)*					
	2.0	5.0	10.5	11.75	16.0	19.0
Power Schedule 1a	3.00	2.50	1.50	1.25	0.80	0.50
Power Schedule 2a	-0.50	-0.75	-1.10	-1.25	-2.00	-2.50
Combined	2.50	1.75	0.40	0.00	-1.20	-2.00
Fractional Change†	0.17	0.30	0.73	1.0	0.4	0.2

*Value of r is the distance from the full-scale experiment with power schedule 1a to that with power schedule 2a. The direction of positive displacement is away from the full-scale experiment with power schedule 1a.

†Fractional Change $= \left| \frac{u_r(\text{nearest experiment}) - u_r(\text{combined})}{u_r(\text{nearest experiment})} \right|$

in a nuclear waste repository, one must not rely solely on mining experience, but also consider the thermomechanical interaction.

4.2 Time-scaled experiment

A right-handed Cartesian coordinate system, Fig. 3 [D3], has been adopted in the thermal calculations for the time-scaled experiment. The mid-plane of the heater array has been chosen as the z = 0 plane with positive z in the upward direction. The x and y axes correspond to the long and short axes of the array, respectively.

Only one power schedule, Fig. 4 [D4], and one physical arrangement of heaters, Fig. 3 [D3], have been considered. Since the heater drift in the time-scaled experiment is 10 m above the midplane of the heater array, it is not expected to significantly influence the temperature field. Accordingly, the host rock is idealized as an infinit medium.

The results have been illustrated as incremental temperature profiles and contour plots. In view of the symmetry that follows from the heater array configuration and the assumptions stated in Section 3.1, results have been plotted only for the positive quadrant of the x-y plane. Figure 22 [D31a] shows the locations of the points for which temperature profiles have been plotted. Points A1-A9 lie on the x-axis, points B1-B8 lie on the y-axis, and points C1-C13 lie on a diagonal of the array passing through a secondary heater. The following points lie on the edge of a heater hole: A1, A5, A6, B1, B5, B6, C1, C5, and C6. The points most distant from the heaters are A9, B8, and C13. Appendix D contains a complete set of temperature profiles.

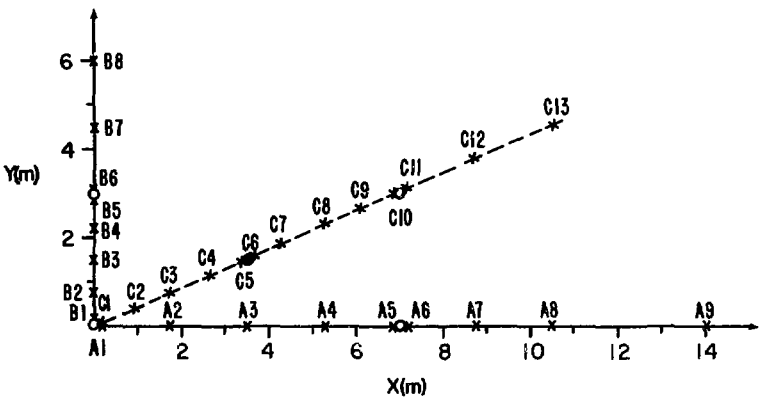

○ PRIMARY HEATERS, ENERGIZED AT THE START OF EXPERIMENT.

● SECONDARY HEATERS, ENERGIZED TWO YEARS AFTER THE START OF EXPERIMENT.
(Heaters not drawn to scale).

XBL 768-2014

Figure 22 Quarter Plane Showing Locations at Which Temperature Profiles Were Made, Hanford Time-Scaled Experiment

Due to the low thermal diffusivity of Pomona basalt, the heat diffuses so slowly away from the heaters that only one meter away from any of the primary heaters, the temperature rise is about 75°C at the end of the first year, 80°C at the end of the second year, and 110°C at the end of the third year. Even at a distance of 0.5 m from any heater, the maximum temperature rise is only about 200°C (Fig. 24d [D32k]). Therefore, in contrast to the full-scale experiments, instrument failure due to high temperatures is unlikely outside of that 0.5-m radius.

The highest temperature reached at the end of three years is 400°C at the edge of the heater holes (Fig. 23b [D31i]). Seventy-five percent of this value is reached within the first 10 days of the experiment, but the temperature does not reach 360°C (90%) until 400 days have elapsed.

The effect of energizing the secondary heaters at the end of two years is apparent in most of the temperature profiles shown in Appendix D. For locations more than 1.5 m away from the secondary heaters (Fig. 23a [D31b]), the effect appears as nothing more than a small increase in the gradient after the two-year mark, whereas at closer locations, such as A3, C4 (Fig. 23b [D31i]), and C7, the temperature increases quite rapidly.

The contour plots in Figs. 24a-24h [D32a,D32c-D32g,D32j,D32k] show the temperature distribution at selected times during the time-scaled experiment in a quarter of the heater midplane. (Appendix D contains a complete time series of contour plots.) Again, as for the contour plots of the full-scale experiments, the highest contour

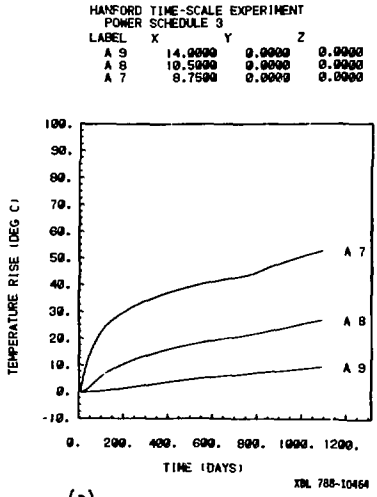

(a)

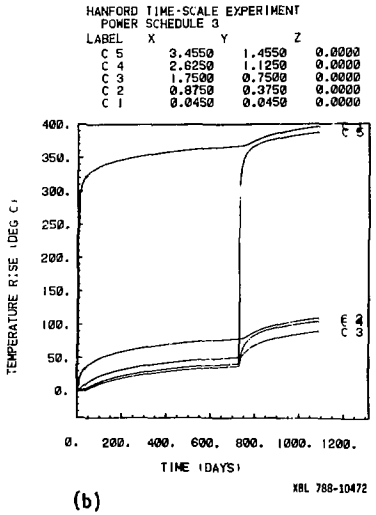

(b)

Figure 23 Temperature Profiles for Hanford Time-Scaled Experiment

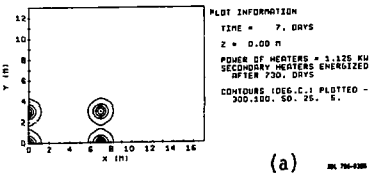

(a)

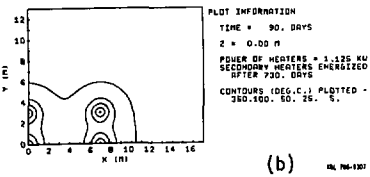

(b)

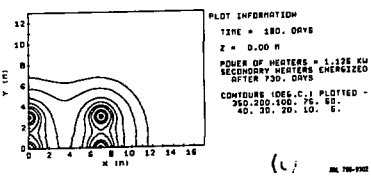

(c)

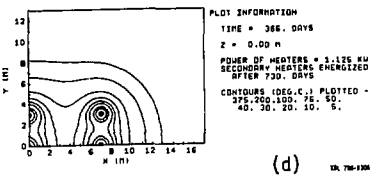

(d)

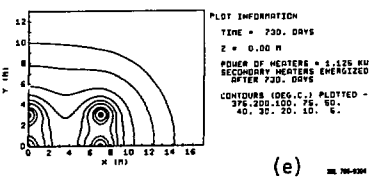

(e)

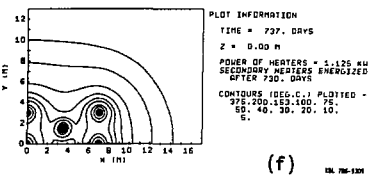

(f)

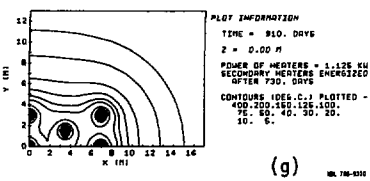

(g)

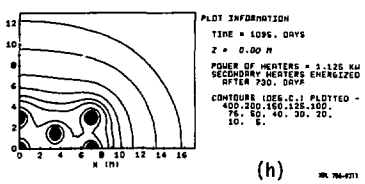

(h)

Figure 24 Isotherms in Horizontal Plane, Hanford Time-Scaled Experiment, z = 0

value has been chosen to be the temperature rise at the edge of the heater hole and contour levels of 100°, 50°, 20° (or 25°) and 5°C appear in every graph.

The interaction of heaters at a spacing of 3 m is noticeable in the first plot, day 7 of the experiment (Fig. 24a [D32a]). By day 90 (Fig. 24b [D32c]) the 5° incremental isotherm for all of the primary heaters has coalesced. At the end of the first year of the experiment the 5° isotherm has become nearly elliptical in shape, intersecting the x-axis at 13 m and the y-axis at 8 m (Fig. 24d [D32e]). During the next year the 5° isotherm moves away from the heaters nearly two meters in both the x and y directions (Fig. 24e [D32f]). Further interaction among the primary heaters can be recognized as the merging of the 10°C and 20°C isotherms between heaters 7 m apart, and 40°C and 50°C isotherms between heaters 3 m apart after 180 and 365 days (Figs. 24c,24d [D32d,D32e]). Only slight changes occur between 365 and 730 days (Figs. 24d,24e [D32e,D32f]), suggesting that the initial test period may either be shortened or else considerably lengthened.

Figure 24f [D32g] shows the predicted temperature distribution one week after the secondary heaters have been energized. The interaction betwen the primary and secondary heaters at the 40°C level has already taken place. Interaction between secondary heaters can be seen from the shape of the 75° isotherms on day 910 (Fig. 24g [D32j]). By the end of the experiment (Fig. 24h [D32k]), the 75° isotherm has irregularly surrounded all of the heaters shown, and the 5° isotherm has moved another two meters away from the heaters. The 100° isotherm is still contained within a one-meter radius of each heater.

Figure 25 [D33] summarizes the migration of the 5° isotherm during the experiment.

An important feature of a planar waste repository is that the rock around the waste canisters near the edge of the repository is cooler than near the center. This will indeed be simulated by the time-scaled experiment, at least qualitatively, in spite of the modest number of heaters used.

In the calculations presented above for the time-scaled experiment, the heaters were assumed to have constant power. If a decaying power is used to simulate heat generation from radioactive waste, the temperature will reach a peak value and then start declining. This has been found to be the case in the predicted temperature rise for a similar time-scaled experiment at Stripa, Sweden (Chan and Remer, 1978). For decaying sources the maximum rock temperature reached at the edge of the heater hole will be about the same, but the maximum temperatures further away from the individual heaters will be lower than those presented here for constant heat sources.

Sequential loading of nuclear waste canisters does appear to be viable in so far as it does not lead to gross temperature increases at local hot spots. Thermomechanical interaction among heaters, however, occurs over a longer distance (see Section 4.1) because it depends on the temperature distribution in the whole region as well as thermal gradients. Finite element calculations of thermally induced displacements and stresses for the time-scaled experiment should be carried out using a three-dimensional model similar to that developed at LBL for the Stripa experiment.

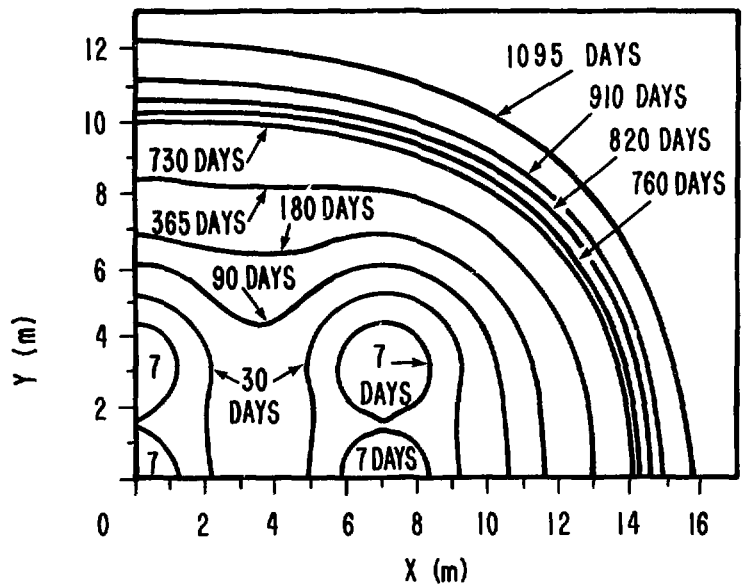

PLOT INFORMATION
Z = 0(m)
Power of heaters = 1.125 kW
Secondary heaters energized
after 730 days. (Contours (days) shown).

XBL 788-2014A

Figure 25 Migration of 5° Isotherm in Horizontal Plane, Hanford Time-Scaled Experiment.

5. SUMMARY, CONCLUSIONS AND RECOMMENDATIONS

Temperatures as well as thermally induced displacements and stresses in the rock have been calculated for the heater experiments in the Near Surface Test Facility at Hanford. Temperatures were obtained by numerically integrating closed form solutions of the heat conduction equation while displacements and stresses were obtained by means of linear thermoelastic finite-element analysis.

For the temperature calculations six different power schedules were considered for the full-scale experiments with initial central heater power ranging from 1 kW to 5 kW and peripheral heater power of either 0.5 kW or 1 kW each. Two of these cases, one with a 5-kW central heater and the other with a 2-kW central heater, were selected for thermomechanical modeling. One case was considered for the temperature calculation of the time-scaled experiment, i.e., with 1.125-kW power per heater.

The calculations indicate that the temperature of the rock adjacent to the full-scale central heater rapidly increases above the ambient, approaching a quasi-steady state in about 60 days after its power has been turned on or stepped up. A ring of eight 1-kW peripheral heaters evenly distributed in a 0.9-m radius circle raises the temperature of the rock within this circle uniformly by 200°C in less than a month without introducing an additional thermal gradient, thus simulating the thermal interaction effect of neighboring canisters in a nuclear waste repository. The temperature increase in the rock due to these peripheral heaters one year after they have been energized

is 250°C. This represents an unacceptably high ambient temperature rise in a repository situation.

Because of the poor thermal conductivity of Pomona basalt (Gable Mountain, Hanford, Washington), very high temperatures are expected. Assuming the heaters to continue functioning and the thermal properties of the rock to remain constant, it has been predicted that maximum temperature rise in the rock at the end of the first, second, and third years will be 440°C, 690°C, and 1270°C for the highest power considered and 85°C, 210°C and 775°C for the lowest power. Consequently, the stressmeters, extensometers and heater (in approximately that order) within 1 m of the 5-kW central heater may fail during the first year of the test. If the central heater is operated at 1 kW, then most of the instruments will survive the two-year test period before the heater power is stepped up.

In the time-scaled experiment the wall of the heater hole reaches 300°C in the first 10 days but never exceeds 400°C throughout the three-year test period. Switching on the secondary heaters increases the temperatures near a primary heater by only about 30°C. At a radial distance of 0.5 m from any heater the rock temperature rises by less than 200°C above the ambient at any time of the test. Consequently, instrument failure is unlikely outside that 0.5-m radius.

The thermal interaction among adjacent heaters is significantly affected by center-to-center spacing.

Comparison between the temperature fields of the full-scale and the time-scaled experiments shows that the concept of scaling is correct.

Maximum radial displacements u_r in each full-scale experiment occur in the midplane of the heater array at radial distances of 1 to 2 m from the center line of the central heater. Maximum values of u_r at the end of the first, second, and third years were predicted to be 0.8 mm, 2 mm and 3 mm for the 5-kW experiment. Maximum vertical displacements are about twice as large as the maximum radial displacements. Both the heater drift and extensometer drift have non-negligible effects on the displacements, especially during the later stages of the experiments and, therefore, the presence of these drifts must be taken into account in the interpretation of the field data.

Highest compressive axial (σ_θ) stresses occur at the wall of the central heater hole. For both power schedules (5-kW or 2-kW central heater) considered in the thermomechanical calculations the maximum values of these compressive stresses during the first two years of the full-scale experiments lie within the range of values for the uniaxial compressive strength of Pomona basalt as determined in small intact specimens in the laboratory. Consequently, descrepitation of the heater hole is likely to occur. At the beginning of the experiment both σ_z and σ_θ are tensile with values of about 1 MPa over a short range of radial distances near the central heater. The highest tensile stresses (σ_r and σ_θ), however, occur just beneath the floor of the heater drift. Again these tensile stresses exceed the laboratory values for the tensile strength of the rock, indicating that cracking of the floor may occur if the rock mass is behaving as a linear elastic continuum.

The thermomechanical analysis reported here is based on continuum models. In a fractured rock mass such as the Pomona formation the discontinuities may accommodate part of the thermal expansion and the displacements and stresses would then be reduced.

Interference between the two full-scale experiments separated by 21 m is negligible with regard to temperatures, significant with regard to displacements and moderate with regard to stresses. Hence, in the interpretation of the thermomechanical response both experiments have to be considered together, especially during the later stages of the tests.

Based on the results of the present analyses the following recommendations can be made:

1. One of the full-scale experiments may be run with the central heater at 5 kW and the peripheral heaters at 1 kW as a "test to failure." The period between energizing the central heater and peripheral heaters may be shortened to about 6 months. The passive microseismic detection technique would be very useful in determining both the time and location for occurrence of thermally induced cracking.
2. The other full-scale experiment should be run with the central heater at 1-2 kW and the peripheral heaters at 0.5 kW, so that sufficient data on the thermomechanical response of the Pomona formation can be collected before the instruments fail.

3. The convergence between the floor and roof of the full scale heater drift can be measured with extensometers. This may facilitate the determination of the amount of floor heave prior to the occurrence of tension fractures on the floor. The information would be useful for repository design as well as monitoring during the operating phase. In a repository, it may be necessary to place the waste canisters in deeper drillholes to mitigate the effects of tension fractures.
4. In view of the low thermal conductivity of Pomona basalt, unless the results of the heater experiments indicate otherwise, it would be prudent to limit the initial power density of any spent fuel canister emplaced underground to 0.4 kW/m (corresponding to a 1-kW full-scale heater of 2.5-m length) to ensure that the temperature of the fuel cladding does not exceed 200°C.
5. The interference between the two full-scale experiments should be taken into account in the analysis of the displacement and stress data.
6. A few extensometers should be placed near the midpoint of the center-to-center line of the two full-scale heaters to assess the thermomechanical interaction.
7. Further temperature calculations should be carried out for the time-scaled heater experiments using the finite source model adopted in this report with decaying sources.

8. Detailed thermomechanical modeling taking into account the discontinuities in the rock should be carried out. To provide meaningful inputs for such models the thermal and mechanical properties and their temperature and time dependency should be measured in situ as well as in large rock samples containing fractures. Furthermore, the fracture pattern of the site has to be mapped out in detail.
9. Since the temperature fields in all of these heater experiments are localized, it is necessary to carry out larger scale heater experiments to investigate thermomechanical response on an excavation and repository scale.

REFERENCES

Agapito, J. F. T., Hardy, M. P., and St. Laurent, D. R., "Geo-Engineering Review and Proposed Program Outline for the Structural Design of a Radioactive Waste Repository in Columbia Plateau Basalts," Report RHO-ST-6, Rockwell Hanford Operation, September 1977.

Ayatollahi, M. S., "Stress and Flow in Fractured Porous Media." Ph. D. Thesis, Department of Material Science and Mineral Engineering, University of California, Berkeley, 1978.

Ayatollahi, M. S., Chan, T., and Witherspoon, P. A., "A Numerical Method for Analysis of the Thermoelastic Behavior of Saturated Fractured Rock Masses," presented at the Second International Conference on Computational Methods in Nonlinear Mechanics, Austin, Texas, March 26-29, 1979.

Bathe, K. J., Wilson, E. L. and Peterson, F. E., "SAPIV, a Structural Analysis Program for Static and Dynamic Response of Linear Systems." Report EERC 73-11, College of Engineering, University of California, Berkeley, June 1973, Revised April 1974.

Carslaw, H. S. and Jaeger, J. C., Conduction of Heat in Solids (Oxford University Press, 1959).

Chan, T., "Thermal and Stress Analyses for a High-Level Radioactive Waste Repository in Crystalline Rock," AECL-5980, Atomic Energy of Canada, Ltd., 1979. First published in October 1977 as a classified report, WNRE-365, Whiteshell Nuclear Research Establishment, Canada.

Chan, T. and Ballentine, L. E., "The Energy Distribution of Electronic States in a Liquid Metal," Physics and Chemistry of Liquids 2, 165 (1971).

Chan, T. and Cook, N. G. W., "Calculated Thermally Induced Displacements and Stresses for Heater Experiments at Stripa," Lawrence Berkeley Laboratory Report, LBL-7061, 1979, in preparation.

Chan, T., Cook, N. G. W., and Tsang, C.-F., "Theoretical Temperature Fields for the Stripa Heater Project," Lawrence Berkeley Laboratory Report, LBL-7082, 1978.

Chan, T. and Remer, J. S., "Semi-Analytic Thermal Calculations for Arrays of Nuclear Waste Canisters Buried in Rock," presented at Am. Geophys. Union 1978 Fall Meeting, December 4-8, 1978, San Francisco, Abstract T75, EOS 59, 1189.

Cook, N. G. W. and Hood, M., "Full-Scale and Time-Scaled Heating Experiments at Stripa: Preliminary Results," presented at the OECD Seminar on In-Situ Heating Experiments in Geological Formations, Stripa, Sweden, September 12-15, 1978; Lawrence Berkeley Laboratory Report, LBL-7072, SAC-11, December, 1978.

Cook, N. G. W. and Witherspoon, P. A., "In Situ Heating Experiments in Hard Rock: Their Objectives and Design," presented at the OECD Seminar on In-Situ Heater Experiments in Geological Formations, Stripa, Sweden, September 12-15, 1978.

Du Bois, A., Binnall, E., Chan T., McEvoy, M., Nelson, P., and Remer, J., "Heater Test Planning for the Near Surface Test Facility at the Hanford Reservation," Lawrence Berkeley Laboratory Report, LBL-8730, 1979.

Duvall, W. I., Miller, R. J., and Wang, F. D. "Preliminary Report on Physical and Thermal Properties of Basalt, Drill Hole DC-10, Pomona-Flow Gable Mountain," Report RHO-BWI-C-11, Earth Excavation Institute, Colorado School of Mines, May 1978.

Ekren, E. B., Dinwiddie, G. A., Mytton, J. W., Thordarson, W., Wier, J.E. Jr., Hinricks, E. N., and Schroeder, W., "Geologic and Hydrologic Considerations for Various Concepts of High-Level Waste Disposal in the Coterminous U. S." U. S. G. S. Open File Report 74-158, 219 pp., 1974.

Gale, J. E., Taylor, R. L., Witherspoon, P. A., and Ayatollahi, M. S., Flow in Rocks with Deformable Fractures, Proceedings Int. Symposium on Finite Element Methods in Flow Problems, Swansea, United Kingdom. University of Alabama at Huntsville Press, 1974.

Goodman, R. E., Methods of Geological Engineering in Discontinuous Rocks (West Publishing Co., St. Paul, 1976).

Goodman, R. E., Taylor, R. L., and Brekke, T. L., "A Model for the Mechanics of Jointed Rocks." Journal of Soil Mechanics and Found. Division, ASCE, vol. 94, no. S. M. 3, 1968.

Haimson, B. C., Report on Hydrofracturing Tests for In Situ Stress Measurements, Near Surface Test Facility, Hole DC-11, Hanford Reservation. Prepared for Lawrence Berkeley Laboratory, September, 1978. Appendix of this report is under separate cover.

Jackson, J. D., Classical Electrodynamics, 2nd Edition (John Wiley and Sons, Inc., New York, 1975).

Jenks, G. H., "Maximum Acceptable Temperatures of Wastes and Containers During Retrievable Geologic Storage," report Y/OWI/TM-42, Office of Waste Isolation, Oak Ridge, August 1977.

Llewellyn, G. H., "Prediction of Temperature Increases in a Salt Repository Expected from the Storage of Spent Fuel or High Level Waste, Oak Ridge National Laboratory Report, ORNL/ENG/TM-7, April, 1978.

Martinez-Baez, F., and Amick, E. H., Thermal Properties of Gable Mountain Basalt Cores, Hanford Nuclear Reservation. Lawrence Berkeley Laboratory Report, LBL-7038, 1979.

Morse, P. M., and Feshbach, H., Methods of Theoretical Physics (McGraw-Hill, New York, 1953).

Noorishad, J., Witherspoon, P. A., and Brekke, T. L., "A Method for Coupled Stress and Flow Analysis of Fractured Rock Masses," Publication no. 71-6, Department of Civil Engineering, University of California, 1971.

Presnall, D. C., Simmons, C. L., and Porath, H., "Changes in Electrical Conductivity of a Synthetic Basalt during Melting," J. Geophys. Res. 77, No. 29, 5665-5672, 1972.

Rockwell Hanford Operations, "In Situ Heater Experiment Plan," unpublished document, July 1978.

Sackett, S., "New Version of SAPIV," unpublished memorandum, MDG 78-14, Lawrence Livermore Laboratory, February, 1978.

APPENDIX A. CLOSED FORM INTEGRAL SOLUTIONS FOR TEMPERATURE DISTRIBUTIONS DUE TO A FINITE CYLINDER AND A DISC SOURCE WITH ARBITRARY TIME DEPENDENCE

Green's Function Method

A general technique to obtain closed form representations of the solutions to nonhomogeneous linear partial differential equations with homogeneous or nonhomogeneous boundary conditions is the Green's function method. It can be shown (Morse and Feshbach, 1953) that the solution to the heat diffusion with prescribed nonhomogeneous boundary and initial conditions is given formally by

$$T(\underline{r},t) = \frac{1}{k}\int_0^t\int_{V_o} Q(\underline{r}',t')\, G(\underline{r},t;\underline{r}',t')\, dV'\, dt' \qquad (A1)$$

$$+ \frac{1}{\kappa}\int_V T(\underline{r}',0)\, G(\underline{r},t;\underline{r}',0)\, dV'$$

$$+ \int_0^t\int_S \left[\nabla' T(\underline{r}',t')\, G(\underline{r},t;\underline{r}',t') - \nabla' G(\underline{r},t;\underline{r}',t')\, T(\underline{r}',t')\right] dS'\, dt'$$

where Q = heat generation rate per unit volume,

V_o = volume occupied by the distributed source,

V = volume over which solution is sought,

S = boundary surface,

G = Green's function.

and the other symbols are the same as defined in Section 3.1. For our present application (solution in an infinite or semi-infinite medium) we need only the first term representing the temperature field caused by a continuous distributed source. The second and third (boundary integral) terms representing the effects of initial and

boundary conditions are included here in anticipation of future applications.

The Green's function in an infinite domain, or the temperature rise $G(\underline{r},t;\underline{r}',t')$ at position $\underline{r}$ at time t due to an impulse source of strength k at $\underline{r}'$ at time t' is

(A2)

$$G(\underline{r},t;\underline{r}',t') = \frac{1}{8k^{1/2}\,[\pi(t-t')]^{3/2}} \exp\left[-\frac{|\underline{r}-\underline{r}'|^2}{4\kappa(t-t')}\right] H(t,t')$$

where $\underline{r} = (x,y,z)$,

$\underline{r}' = (x',y',z')$,

$H(t,t') = 0$, $t < t'$

$= 1$, $t > t'$,

is the Heaviside step function.

Finite Cylinder Source

For a cylindrical heat source of radius a, height 2b and heat generation rate per unit volume $Q_c(t)$, oriented along the z-axis with its midpoint at the origin, the temperature rise can be obtained by substituting Eq. (A2) into the first term of Eq. (A1). Transforming to cylindrical polar coordinates and utilizing the properties of the error function and Bessel functions, one arrives at the following two alternative expressions,

$$\Delta T(r,z,t) = \frac{1}{4k}\int_0^t \frac{Q_c(t-\mu)}{\mu}\left[\operatorname{erf}\left\{\frac{z+b}{2(\kappa\mu)^{1/2}}\right\} - \operatorname{erf}\left\{\frac{z-b}{2(\kappa\mu)^{1/2}}\right\}\right] \int_0^a e^{-\frac{(r^2+r'^2)}{4\kappa\mu}} I_0\left(\frac{rr'}{2\kappa\mu}\right) r'dr'd\mu \qquad \text{(A3)}$$

or

$$\Delta T(r,z,t) = \frac{\kappa a}{2k}\int_0^t Q_c(t-\mu)\left[\operatorname{erf}\left\{\frac{z+b}{2(\kappa\mu)^{1/2}}\right\} - \operatorname{erf}\left\{\frac{z-b}{2(\kappa\mu)^{1/2}}\right\}\right] \int_0^\infty e^{-\kappa\mu\alpha^2} J_0(\alpha r)\, J_1(\alpha a)\, d\alpha d\mu \qquad \text{(A4)}$$

where $r = (x^2 + y^2)^{1/2}$, $r' = (x'^2 + y'^2)^{1/2}$.

Our expressions (A3) and (A4) are essentially identical to those given by Mufti (1971) except that, whereas he assumed an exponentially decaying source, we have retained the source function in the integrand so that our expressions are valid for any arbitrary time dependence. Since we are going to evaluate the integrals by *numerical* quadrature, it is *unnecessary* to assume *any* particular functional dependence. As noted by Hodgkinson (1977) the form (A3) is far more convenient for numerical evaluation than the form (A4) since the latter involves the product of two oscillatory functions J_0 and J_1 in the integrand. A Fortran program CYNDER based on Eq. (A4) has previously been developed by Chan and used for verifying the line source approximation (Chan et al., 1978).

Disc Source

The temperature field caused by a disc source can be obtained as a special case of (A3) by taking the limit $b \to 0$ or directly from

Eqs. (A1) and (A2), integrating over the disc instead of the cylinder. The result is

$$\Delta T(r,z,t) = \frac{1}{4k(\pi\kappa)^{1/2}} \int_0^t \frac{Q_d(t-\mu)}{\mu^{3/2}} \int_0^a \exp\left[-\frac{r'^2 + r^2 + (z-z')^2}{4\kappa\mu}\right] I_0\left(\frac{rr'}{2\kappa\mu}\right) r'dr'd\mu \qquad (A5)$$

where Q_d = heat generation rate for unit area of the disc. Equation (A5) is useful for long-term repository and regional scale studies.

REFERENCES

Chan, T., Cook, N. G. W., and Tsang, C.-F., "Theoretical Temperature Fields for the Stripa Heater Project," Lawrence Berkeley Laboratory Report, LBL-7082, 1978.

Hodgkinson, D. P., "Deep Rock Disposal of High Level Radioactive Waste: Transient Heat Conduction from Dispersed Blocks," AERE-R8763, June, 1977.

Morse, P. M., and Feshbach, H., Methods of Theoretical Physics (McGraw-Hill), New York, 1953).

Mufti, I. R., "Geothermal Aspects of Radioactive Waste Disposal into the Subsurface," J. Geophys. Res. 76, 8568, 1971.

APPENDIX B. GENERALIZATION TO AN ANISOTROPIC MEDIUM

Anisotropy may occur in the rock material because of preferred orientation of the mineral crystals, and in the rock mass because of preferred orientation of foliation planes or joint sets. In an anisotropic medium with principal thermal conductivities k_1, k_2, k_3 in the direction of the x, y, and z-axes, Eqs. (A1) and (A2) can be generalized to

$$T(\underline{r},t) = \frac{1}{(k_1k_2k_3)^{1/3}} \int_0^t \iiint_{V_o} Q(\underline{r}',t')\, G(\underline{r},t;\underline{r}',t')\, dV'dt' + \frac{\rho c}{(k_1k_2k_3)^{1/3}} \iiint_V T(\underline{r}',o)\, G(\underline{r},t;\underline{r}',o)\, dV' + \int_0^t \iint_S [\nabla' T(\underline{r}',t')\, G(\underline{r},t;\underline{r}',t') - \nabla' G(\underline{r},t;\underline{r}',t)\, T(\underline{r}',t')]\, dS'dt' \tag{B1}$$

with

$$G(\underline{r},t;\underline{r}',t') = \frac{(\rho c)^{1/2}}{8(k_1k_2k_3)^{1/6}\,[\pi(t-t')]^{3/2}} \exp\left[-\frac{\rho c}{4t}\left\{\frac{(x-x')^2}{k_1} + \frac{(y-y')^2}{k_2} + \frac{(z-z')^2}{k_3}\right\}\right] \cdot H(t,t') \tag{B2}$$

where ρ = density,

c = specific heat per unit mass.

The expression (B2) is essentially the same as that given by Carslaw and Jaeger (1959).

Evidently having redefined the length scales such that

$$\frac{x^2}{(k_1k_2k_3)^{1/3}} = \frac{x^2}{k_1} \quad , \quad \frac{y^2}{(k_1k_2k_3)^{1/3}} = \frac{y^2}{k_2} \quad , \quad \frac{z^2}{(k_1l_2k_3)^{1/3}} = \frac{z^2}{k_3} \quad ,$$

all the equations in Section 3.1 and Appendix A can be generalized with minor changes in terms involving the thermal properties.

REFERENCE

Carslaw, H. S. and Jaeger, J. C., Conduction of Heat in Solids (Oxford University Press, 1959).

APPENDIX C. CONSIDERATION OF TEMPERATURE RISE AS A FUNCTION OF THE GROUP PARAMETER t/r^2; COMPARISON OF FINITE LINE AND INFINITE LINE SOURCES

It is frequently useful to examine a solution of the conduction equation as a function of a group parameter. An appropriate choice for the heat diffusion equation would be t/r^2. In this case, however, the calculated temperature rise is not a function of t/r^2 as can be seen from Fig. C1 or from the solution itself, Eq. (3), Section 3.1.

Figure C1 shows a log-log plot of temperature rise vs t/r^2. Four of the curves shown are based on temperature calculations made for power schedule 1a for points in the heater midplane ($z = 0$). Each of those lines represents a different value of radial distance (r = 0.229, 0.5, 1, 2 m) and the points on each line correspond to different time values.

The solid curve in Fig. C1 corresponds to the temperature rise generated by a constant infinite line source:

$$\Delta T(r,t) = \frac{Q_1}{4\pi k} \int_0^t \frac{1}{\mu} \exp\left(\frac{-r^2}{4\mu\kappa}\right) d\mu \quad ,$$

where Q_1 = heat output per unit length (W/m),

k = thermal conductivity (W/m°C),

κ = thermal diffusivity (m^2/day),

t = time (days),

r = radial distance (m).

This expression was obtained by finding the limit as $b \to \infty$ of the expression in Eq. (3), Section 3.1. Alternatively, it can also be

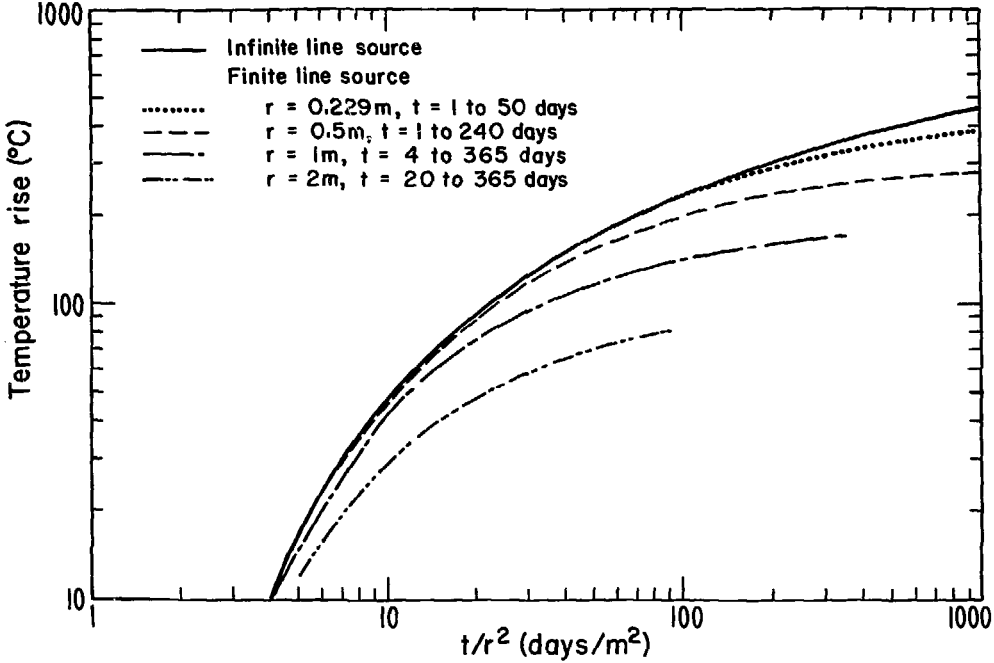

Figure C1 Comparison of Temperature Profiles for Infinite and Finite Line Sources

derived by evaluating Eq. (A1) in Appendix A directly using the proper integration limits (Carslaw and Jaeger, 1959).

The temperature rise due to an infinite line source is in fact a function of the group parameter t/r^2 as can be shown by the following change of variables. Let

$$\lambda = \frac{r^2}{4\mu\kappa} \quad ,$$

then

$$d\mu = \frac{-r^2}{4\lambda^2\kappa} \, d\lambda \quad .$$

The lower limit of integration for the integral in μ is 0, the upper limit is t, corresponding to a lower limit of $+\infty$ and an upper limit of $r^2/4t\kappa$ for the integral in λ. Finally,

$$\frac{Q_1}{4\pi k} \int_0^t \frac{1}{\mu} \exp\left(\frac{-r^2}{4\mu\kappa}\right) d\mu = \frac{Q_1}{4\pi k} \int_\infty^{r^2/4t\kappa} -\frac{e^{-\lambda}}{\lambda} \, d\lambda \quad ,$$

$$= \frac{Q_1}{4\pi k} \int_{r^2/4t\kappa}^\infty \frac{e^{-\lambda}}{\lambda} \, d\lambda \quad ,$$

$$= \frac{Q_1}{4\pi k} \, E_1\left(\frac{r^2}{4\kappa t}\right) \quad .$$

The function E_1 is one form of the exponential integral, frequently tabulated in mathematical handbooks, e.g., Abramowitz and Stegun (1964).

For small values of time and short distances away from the central heater, the solution corresponding to a finite line source resembles that of an infinite line source because points on the line source

far away from the midplane contribute little to the temperatures at the field points considered. This is illustrated in Fig. C1 by the coincidence of the curves corresponding to the two different solutions.

REFERENCES

Abramowitz, M. and Stegun, I. A., Handbook of Mathematical Functions, (National Bureau of Standards, 1964).

Carslaw, H. S., and Jaeger, J. C., Conduction of Heat in Solids (Oxford University Press, 1959).

APPENDIX D. COMPLETE SET OF FIGURES

Appendix D, contained in Volume 2, is a complete set of figures illustrating the detailed results necessary for the design of the heater experiments at the Near Surface Test Facility at Hanford. Table D1, given here, summarizes the type of calculations made (temperature, displacement, or stress) for the power schedules and mathematical models considered. A list of the figure numbers in this appendix corresponding to figures in the text is given in Table D2.

Table D1. Summary of figures representing models studied.

(a) Full-Scale Experiments

	Temperature Calculations		Displacement Calculations		Stress Calculations	
Power Schedule	Infinite Medium	Isothermal Boundary	Mesh 1	Mesh 7	Mesh 1	Mesh 7
1a (Fig. 2a)	D6a,D7a D8a-D8m	D9a-D9m	D12a,D12b D14a,D14b D15a,D15b D16a,D16b D20a-D20l	D12a,D12b D17a,D17b D18a,D18b D19a,D19b D22a,D22b	D24a-D24m	D26a,D26b,D27a,D27b
1b (Fig. 2b)	D6b,D7b					
1c (Fig. 2c)	D6c,D7c					
2a (Fig. 2d)	D6d,D7d D10a-D10m	D11a-D11m	D13a,D13b D14a,D14b D15a,D15b D16a,D16b D21a-D21l	D13a,D13b D17a,D17b D18a,D18b D19a,D19b D23a,D23b	D25a-D25m	D26a,D26b,D27a,D27b
2b (Fig. 2e)	D6e,D7e					
2c (Fig. 2f)	D6f,D7f					
Interference between Experiments with 1a (Fig. 2a) and 2a (Fig. 2d)	D28a,D28b		D30a,D30b		D29a,D29b	

(b) Time-Scaled Experiment

3 (Fig. 4)	D31a-D31h D32a-D32k D33					

Table D2. Correspondence between figures in Volume 1 and Appendix D, Volume 2.

Figure Number in Volume 1	Figure Number in Appendix D, Volume 2
1	D1
2a-2f	D2a-D2f
3	D3
4	D4
5a-5c	D5a-D5c
6a-6c	D6a,D6d,D6f
7a-7c	D7a,D7d,D7f
8a,8b	D8e,D8i
9a-9c	D9b,D9e,D9i
10a,10b	D10e,D10i
11a-11c	D11b,D11e,D11i
12a,12b	D12a,D12b
13a-13c	D17a,D18a,D19a
14a-14f	D20b-D20f,D20i
15	D22a
16a-16e	D24a-D24c,D24f,D24g
17	D26a
18	D27a
19	D28a
20	D29a
21	D30a
22	D31a
23a,23b	D31b,D31i
24a,24h	D32a,D32c-D32g,D32j,D32k
25	D33